FERMILAB-PUB-15-274-TD
ACCEPTED

Research and Development of Nb_3Sn Wires and Cables for High-Field Accelerator Magnets

Emanuela Barzi, Alexander V. Zlobin
Fermi National Accelerator Laboratory (FNAL)
Pine and Kirk Roads, Batavia, IL 60510, U.S.
E-mail: barzi@fnal.gov, zlobin@fnal.gov

***Abstract*– The latest strategic plans for High Energy Physics endorse steadfast superconducting magnet technology R&D for future Energy Frontier Facilities. This includes 10 to 16 T Nb_3Sn accelerator magnets for the luminosity upgrades of the Large Hadron Collider and eventually for a future 100 TeV scale proton-proton (*pp*) collider. This paper describes the multi-decade R&D investment in the Nb_3Sn superconductor technology, which was crucial to produce the first reproducible 10 to 12 T accelerator-quality dipoles and quadrupoles, as well as their scale-up. We also indicate prospective research areas in superconducting Nb_3Sn wires and cables to achieve the next goals for superconducting accelerator magnets. Emphasis is on increasing performance and decreasing costs while pushing the Nb_3Sn technology to its limits for future *pp* colliders.**

I. Introduction and Historical Overview

To push the magnetic field in accelerator magnets beyond the Nb-Ti magnets of the Large Hadron Collider (LHC), superconductors with higher critical parameters are needed. Among the many known high-field superconductors Nb_3Sn is sufficiently developed to be presently used in magnets above 10 T. This superconductor is industrially produced in the form of composite wires in long (>1 km) length, as required for accelerator magnets.

The intermetallic compound Nb_3Sn is a type II superconductor having a close to stoichiometric composition (from 18 to 25 at.% Sn) and the A15 crystal structure. It has a critical temperature T_{c0} of up to 18.1 K and an upper critical magnetic field B_{c20} of up to 30 T [1]. As a comparison, the ductile alloy Nb-Ti has a T_{c0} of 9.8 K and a B_{c20} of up to 15 T. Nb_3Sn stronger superconducting properties enable magnets above 10 T. At a world production of more than 400 tons/year, it is the second superconducting material most widely used in large-scale magnet applications. For instance, it is the material of choice for Nuclear Magnetic Resonance (NMR) spectrometers, which have become a key analysis tool in modern biomedicine, chemistry and materials science. These systems use magnetic fields up to 23.5 T, which correspond to a Larmor frequency of 1000 MHz. Nb_3Sn is also used in high field magnets for the plasma confinement in fusion reactors. The International Thermonuclear Fusion Research and Engineering project (ITER, France) includes a Central Solenoid of 13.5 T and a Toroidal Field magnet system of 11.8 T. Some of the challenges are that Nb_3Sn requires high-temperature processing and it is a brittle superconductor, which makes its critical current strain sensitive, i.e. high strain on the sample may reduce or totally destroy its superconductivity.

The A15 crystal structure was first discovered in 1953 by Hardy and Hulm in V_3Si, which has a T_{c0} of 17 K [2]. A year later, Matthias et al. discovered Nb_3Sn [3]. The first laboratory attempt to produce wires was in 1961 by Kunzler et al. [4] by filling Nb tubes with crushed powders of Nb and Sn. The tube was sealed, compacted, and drawn to long wires. This primitive Powder-in-Tube (PIT) technique required reaction at high temperature, in the range of 1000 to 1400°C, to form the superconducting phase. Nevertheless, that same year it was used to fabricate the first 6 T magnet. An initial alternative to the PIT and the first commercial Nb_3Sn production was in 1967 in the form of tapes by surface diffusion process. Benz and Coffin passed a Nb tape through a bath of molten Sn, and reacted the coated tape to form Nb_3Sn. Although successful in demonstrating the use of Nb_3Sn in high-field magnets, neither technique was practical. The large filaments in the case of the PIT wire, and the inherently large aspect ratio of the tape, invariably resulted in large trapped magnetization and flux jump instabilities. In the late 1960s, Tachikawa introduced an alternative concept based on solid state diffusion [5]. This principle has been used to fabricate Nb_3Sn wires by the so-called bronze route [6-7], which is today one of the leading techniques for manufacturing Nb_3Sn.

In the 1980s and 90s conductor development programs for accelerator magnets were focused on Nb-Ti composite wires and were driven by the needs of accelerators such as the Tevatron, the Accelerator and Storage Complex (UNK, former Soviet Union), the Superconducting Super Collider (SSC) and the LHC [8]. The development of Nb_3Sn conductor was mainly steered by fusion magnet programs [9]. It is since the late 1990s that the High Energy Physics (HEP) community has taken leadership in the development of Nb_3Sn wires for post-LHC accelerators, and used these wires for high field accelerator magnet R&D, which has led to magnetic fields beyond the limits of Nb-Ti technology. Among the several manufacturing processes that have been developed to produce superconducting Nb_3Sn wires in addition to the bronze route, there is the Internal Tin technique, which includes as variants

Work supported by Fermi Research Alliance, LLC, under contract No. DE-AC02-07CH11359 with the U.S. Department of Energy.

the Modified Jelly Roll (MJR) and the Restacked Rod Processes (RRP®) [10] by Oxford Instruments – Superconducting Technology (OST), as well as a more sophisticated PIT method [11]. Nb_3Sn properties and fabrication methods have been reviewed elsewhere [10-15].

Accelerator magnets need high-current multi-strand superconducting cables to reduce the number of turns in the coils, and thus magnet inductance. In addition, using multi-strand cables allows limiting the piece length requirement for wire manufacturing which is important for large magnets. To achieve in a cable the required current, several strands have to be connected in parallel and twisted or transposed in the axial direction. The strands in a cable are not insulated from each other to allow current redistribution between strands in the case of localized defects or quenches. There are several different types of cable used in accelerator magnets [16]. The Rutherford cable, developed at the Rutherford Appleton Laboratory (RAL) [17], has played a crucial role in establishing Nb-Ti accelerator magnet technology. It is widely used in modern high energy accelerators and colliders due to its excellent mechanical, electrical and thermal properties. Superconducting dipoles and quadrupoles based on this cable design and on Nb-Ti strands were successfully used in the Tevatron, Hadron-Elektron Ring Anlage (HERA), Relativistic Heavy Ion Collider (RHIC) and LHC [16]. A new generation of accelerator magnets, being developed in the US [18] and in Europe [19], is using Rutherford cables with Nb_3Sn strands.

The next section II of this paper, "Nb_3Sn Composite Wires", briefly describes the existing Nb_3Sn wire technologies and then focuses on identifying parameters that are important for accelerator magnet design and operation. Past and present R&D programs are touched on, as well as Nb_3Sn wire state-of-the-art performance. The following section III on "Nb_3Sn Wire Properties" details those key research activities and methods used in the international community that helped study and solve most of the aspects required of Nb_3Sn wires for magnet realization. The next two sections IV and V on "Nb_3Sn Rutherford Cables" and "Nb_3Sn Rutherford Cable Properties" attempt to do the same for cables, and finally in the "Next Steps and R&D Goals" section we discuss important research topics for Nb_3Sn to help achieve 15 to 16 T accelerator magnet field and cost reduction goals.

II. Nb_3Sn Composite Wires

Requirements of superconductor stability with respect to magnetic flux jumps and superconductor protection in case of transition to the normal state led to the concept of composite superconducting wire, in which thin superconducting filaments are distributed in a normal low resistance matrix [20]. This matrix provides several important functions. It conducts heat away from the surface of the superconducting filaments because of high thermal conductivity, absorbs a substantial fraction of heat due to high specific heat, and decreases Joule heating when the superconductor becomes normal. To reduce the eddy currents induced by varying external fields and improve stability of a composite wire to flux jumps, these filaments are twisted along the wire axis.

In this section, we briefly touch on Nb_3Sn wire technologies, describe the heat treatment cycle and its functions, identify fundamental parameters and properties of Nb_3Sn wires, summarize the most recent conductor R&D programs, and describe commercial wires and their progress.

A. Nb_3Sn Composite Wire Fabrication

Nb_3Sn composite wires are currently produced using three main methods: bronze, internal tin, and powder-in-tube [15].

The bronze process (Br) is based on a large number of Nb filaments dispersed in a Sn-rich bronze matrix. The initial billet is made of hundreds of Nb rods and it is drawn into a hexagonal element of intermediate size. The rods are then cut and assembled in a second billet, which is extruded, annealed and drawn to final wire size. The bronze core is surrounded by a high-purity Cu matrix which is separated by a thin Nb or Ta diffusion barrier. The bronze route provides the smallest filament size (~2-3 μm), but has a relatively low J_c due to the limited Sn content in bronze.

The Internal Tin (IT) process was introduced in 1974 [21] to overcome the limits of the Br method. It is based on assembling a large number of Nb filaments and pure Sn or Sn-alloy rods in a Cu matrix. The assembly is surrounded by a thin Nb or Ta barrier to prevent Sn diffusion into the high-purity Cu matrix, and it is then cold-drawn down to final size. Restacking of assemblies allows further reducing the final subelement size. Due to the optimal amount of Sn this process gives the highest J_c, but limits the minimal subelement size attainable in the final wire. The IT process has several modifications. The most well-known are the MJR [10], Hot Extrusion Process (HER) [22], RRP® [10], Distributed Tin Process (DTP) [23], and Enhanced Internal Tin (EIT) [24]. These modifications differ by the design of the Nb filaments, the diffusion barrier position, the Sn distribution in the composite cross section, subelement and billet processing, etc., and have different potentials and limitations in term of their performance and large scale production. All these details are described in specialized literature.

The Powder-in-Tube (PIT) process is based on stacking thick-wall Nb tubes, filled with fine $NbSn_2$ powder in a high-purity Cu matrix. The stacked assembly is drawn or extruded to final wire size. This method allows an optimal combination of small filament size (<50 μm) and high J_c comparable with the IT process. However, the current cost of PIT wire is 2 to 3 times higher than the IT wire cost.

Important features of practical materials for superconducting accelerator magnets include performance and its reproducibility in long lengths, commercial production and affordable cost. At present the IT RRP® by OST and PIT by Bruker European Advanced Superconductors (Bruker EAS) are the two processes of Nb_3Sn composite wires with sufficiently high J_c for HEP applications that are available in large quantities from industry.

B. Reaction Cycle

In all methods the Nb_3Sn phase is produced during a final high-temperature heat treatment (HT). The HT cycle is characterized by the temperature profile, i.e. temperature dwells, their duration time, and temperature ramp rates. It is

usually optimized for each Nb_3Sn wire type and application. To achieve the highest J_c in Nb_3Sn wires, the HT has to provide the ideal phase stoichiometry and also an optimal Nb_3Sn phase microstructure.

Nb_3Sn is formed by solid diffusion at high temperature (650°C or higher). In the binary Nb-Sn system, single-phase Nb_3Sn form only above ~930°C, where the only stable phase is Nb_3Sn. At temperatures below 845°C, the two non-superconducting phases $NbSn_2$ and Nb_6Sn_5 are also stable and all three phases will grow at the interface, with $NbSn_2$ most rapidly formed and Nb_3Sn being the slowest. However, in the ternary system (Nb-Cu-Sn) the only relevant stable phase is Nb_3Sn even at lower temperatures. The diffusion path from the Cu-Sn solid solution to the Nb-Sn solid solution passes through only the A15 phase field, preventing formation of the non-superconductive phases. In short, the addition of Cu lowers the A15 formation temperature from well above 930°C to any other that is deemed practical, thereby also limiting grain growth and retaining a higher grain boundary density, as required for flux pinning.

1) Reaction of Internal Tin Wires

During HT of IT wires, several Cu-Sn phases are created and eliminated in the course of the Cu-Sn diffusion and Nb_3Sn formation processes. The presence of liquid phases in IT wires may cause motion of Nb filaments, allowing contact with adjacent ones, and the presence of voids may hinder the diffusion process. In addition, wire bursts due to liquid phases overpressure can damage the wires. These problems are solved by using a 3-step HT cycle.

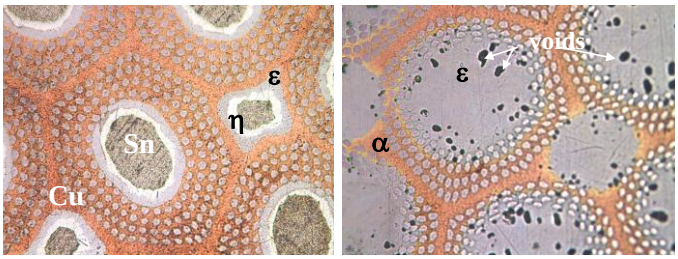

Fig. 1. Intermetallic growth in an IT (IGC) strand after 7 days at 210°C (left), and after 2 days at 400°C (right). Some voids can be seen in the latter [26].

In the first step, temperature dwells below 227°C allow formation of a thin layer of a higher melting point Cu-Sn phase (called also ε phase) that works as a container against the overpressure of the liquid Sn above 227°C. Since the ε phase thickness formed at 210°C after 1 week is only about 1 μm larger than that formed after 3 days, a 3 day 210°C dwell followed by a 1 day at 400°C not only appropriately diffuses the Sn through the Cu, but also prevents Sn leaks. Investigation of the kinetics of phase growth also showed [25] that for temperatures above 440°C, the Cu-Sn δ phase growth is associated with the formation of voids and segregations that may result in cracks along the diffusion path. Since this phenomenon hinders the diffusion process between Cu and Sn, Cu-Sn diffusion in Nb_3Sn wires is performed below 440°C. Fig. 1 shows cross sections of an IT wire by Intermagnetics General Corporation (IGC) at the end of the first two HT steps. After 7 days at 210°C (left), a substantial part of the Sn is still unreacted. After 2 days at 400°C (right) the Sn has been completely converted into ε phase. Some voids are formed in the ε phase during the reaction.

The superconducting Nb_3Sn phase is formed during the third step of the HT cycle between 620 and 750°C. During this stage the optimal phase microstructure, critical for flux pinning, is also formed. The Nb_3Sn microstructure is controlled by the temperature and the duration of this stage. Usually reaction at higher temperature takes the shortest time, but produce the largest grains. The choice of temperature and duration of the third stage is a compromise between optimal pinning structure leading to high J_c and Sn diffusion through the barrier leading to Cu pollution and increase of the matrix electrical and thermal resistivity.

2) Reaction of PIT Wires

In PIT wires the Nb_3Sn A15 phase is formed in a solid state diffusion reaction typically in a few days at ~675°C. The Sn diffusion and Nb_3Sn phase formation processes in the PIT route are visualized in Fig. 2 and described in detail elsewhere [12]. The $NbSn_2$ powder first turns into Nb_6Sn_5 and then in the Nb_3Sn phase. This transitional Nb_6Sn_5 phase is shown in Fig. 2 (left) as the lightest grey area, which surrounds the core after 4 hours at 675°C. After 16 hours, the initial Nb_6Sn_5 phase is converted into large grains. The void fraction in these regions is attributed to the reduced volume of Nb in Nb_3Sn, relative to Nb_6Sn_5 phase. As seen in Fig. 2 (center right), the Nb_3Sn phase formation ends after about 64 hours at 675°C, due to Sn depletion of the core-A15 interface region. Thus, a longer reaction does not increase the Nb_3Sn fraction. The outer boundary of the Nb_3Sn area is controlled to prevent Sn diffusion into the high purity Cu matrix, and the resulting decrease in the Residual Resistive Ratio (*RRR*). The HT of commercial PIT composite wires without a diffusion barrier is optimized with respect to the area of reacted Nb to provide high *RRR* values, typically above 150.

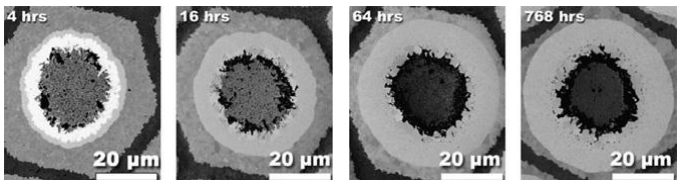

Fig. 2. Reaction progress in the filaments vs. time at 675°C for a ternary 192 filament PIT wire produced by SMI [12].

Heat treatment studies and optimization for IT and PIT wire allowed significant reduction of the reaction time without a substantial degradation of the strand performance. Reduction of reaction time is important for magnet cost saving. Some examples of HT optimization for RRP and PIT wires can be found in [27] and [28].

C. Main Parameters and Properties

The most important technical parameters which define the performance of a composite wire include wire diameter D, critical current density $J_c(B,T)$, magnetization $M(B,dB/dt)$, effective filament diameter d_{eff}, filament twist pitch l_p, superconductor fraction λ or Cu/non-Cu ratio, matrix axial ρ_n

and transverse ρ_e resistivity, and Residual Resistivity Ratio *RRR*. Since Nb_3Sn requires heat treatment, the parameters of the heat treatment cycle are essential to achieve an optimal J_c and *RRR*. Finally, the conductor cost is important too.

The *critical current density* J_c is a key parameter, which controls the current carrying capability, stability, magnetization and AC losses of a superconducting wire, and thus the performance of superconducting magnets. It depends on the superconductor microstructure. The resistive transition of a composite superconductor is smooth, which leads to some uncertainty in the definition of J_c. Several criteria were formulated to define J_c based on resistive transition (or voltage-current characteristic) measurements. The most commonly used criteria for superconducting magnets define J_c at the axial resistivity of 10^{-14} Ω·m, or at a given electric field.

The critical current density, $J_c(B,T,\varepsilon)$, as a function of magnetic field B, temperature T and strain ε, for Nb_3Sn composite wires is parameterized as [29]-[32]:

$$J_c(B,T,\varepsilon) = \frac{C(t,\varepsilon)}{B}(1-t^m)^n b^p (1-b)^q,$$

where:

$b=B/B^*_{c2}(T,\varepsilon)$, $t=T/T_{c0}(\varepsilon)$ and $B^*_{c2}(T,\varepsilon)= B^*_{c20}(0,\varepsilon)\cdot(1-t^v)\cdot k(t)$.

Parameters m, n, p, q, v as well as functions $C(t,\varepsilon)$, $T_{c0}(\varepsilon)$, $k(t)$ and $B^*_{c20}(0,\varepsilon)$ are usually determined by fitting experimental data of Nb_3Sn wires. For the practical strain range of $-1<\varepsilon<0.5$ the experimental data are well fitted with $m=n=q=2$, $p=0.5$, $v=1.7$ to 2 and $C(t,\varepsilon)=C(\varepsilon)$.

One of the practical purposes of parametrization is that of calculating the expected performance of a magnet from I_c measurements of strand samples used as witnesses during coil reaction. The intersection of the critical surface of each coil at the various magnet test temperatures with the B_{peak} load line of the magnet produces the expected coil short sample limit (SSL) current at that temperature.

The *engineering current density* J_E is defined as the critical current density per total conductor cross section. It depends on the superconductor J_c and superconductor fraction λ or Cu to non-Cu ratio r in the composite cross section. The relation between λ and r is as follows:

$$\lambda = \frac{1}{r+1}.$$

Wire *magnetization*. A composite superconductor wire placed in a varying magnetic field becomes magnetized [20] with a magnetization described by the following formula:

$$M(B,\dot{B}) = -\mu_0\left[\frac{2}{3\pi}\lambda J_c(B) d_{sc} + \frac{l_p^2\dot{B}}{4\pi^2\rho(B)}\right],$$

where d_{sc} is the filament diameter, l_p is the filament twist pitch, $\rho(B)$ is the effective transverse resistivity of the matrix, and $J_c(B)$ is the critical current density in the superconductor. The first term represents the component related to persistent currents in the superconducting filaments, and the second term represents the component associated with coupling eddy currents between filaments. Both components are diamagnetic in an increasing field and paramagnetic in a decreasing field. Composite wire magnetization plays an important role in superconducting accelerator magnets [33], which have demanding requirements on field uniformity. It is to be noted that in Nb_3Sn d_{sc} is indicated as d_{eff} (see below), since contrary to Nb-Ti, the filament size is not always identical to its geometric size.

AC losses. Magnetic hysteresis leads to energy dissipation in superconducting composite wires [20]. Similarly to magnetization, the power of AC losses P in a composite superconductor has two main components related to persistent and coupling eddy currents. The AC loss power per unit volume of composite wire after full flux penetration in superconducting filaments can be represented as follows:

$$P(B,\dot{B}) \cong \frac{2}{3\pi}\mu_0\lambda J_c(B) d_{sc}\dot{B} + \frac{\mu_0 l_p^2 \dot{B}^2}{4\pi^2\rho(B)}.$$

AC losses in composite superconductors play an important role in the thermal stabilization of superconducting coils during magnet operation and quench, and contribute to the heat load on a magnet cooling system.

The *effective filament diameter* d_{eff} impacts the level of wire magnetization and its effect on magnet field quality at low fields, as well as conductor stability against flux jumps. The d_{eff} can be obtained from the width of the magnetization loop $\Delta M(B) \propto J_c(B)\cdot d_{eff}$ using a measured $J_c(B)$ dependence. At present, the d_{eff} of Nb_3Sn strands with high J_c is still quite large (~50 to 100 μm to be compared with ~5 μm in Nb-Ti composite wires) for both the IT and the PIT processes. The reduction of d_{eff} is limited in IT and PIT wires by the wire architecture and specifics of the manufacturing processes.

Analysis of *stability* of the superconducting state with respect to small field or temperature perturbations [20] has led to the following adiabatic stability criterion for the maximum transverse size d_{max} of a hard Type II superconductor:

$$d_{max} < \frac{\pi}{2}\sqrt{\frac{C_p(B,T)\cdot(T_c(B)-T_b)}{\mu_0 J_c(B)^2\cdot(1+3i)}}$$

where $C_p(B,T)$ is the superconductor specific heat, $J_c(B)$ and $T_c(B)$ are the superconductor critical parameters, T_b is the helium bath temperature and i is the ratio of transport current I_T to critical current I_c. Thus, for all practical Nb_3Sn composite wires with d_{eff} ~50 to 70 μm, as presently used in accelerator magnets, the above stability criterion predicts flux jump instabilities at low fields.

The *wire diameter D* defines the critical current I_c that the wire can carry and thus the number of turns in a magnet. Flux jumps limit not only the size of the superconducting filaments but also the size of a multifilament composite wire due to self-field instability. The typical value of D for IT and PIT wires at present is 0.5 to 1.0 mm. The adiabatic *self-field stability* criterion [20] sets the following upper limit for the composite wire diameter D_{max}:

$$D_{max} < \sqrt{\frac{32 C_p(B,T)\cdot(T_c(B)-T_b)}{\mu_0\lambda J_c(B)^2(-2\ln(1-i)-2i-i^2)}},$$

where λ is the fraction of superconductor in the wire cross section, $C_p(B,T)$ is the wire specific heat, and i is the ratio of transport current I_T to critical current I_c. This criterion also

predicts self-field flux instabilities in practical Nb_3Sn composite wires.

The *specific heat C_p* of a superconductor and a composite wire plays an important role by not only limiting flux jump instabilities in the superconducting filaments and in the composite wire, but also by improving the superconductor quench protection by controlling its temperature during a quench. The $C_p(B,T)$ of a Nb_3Sn composite wire is defined by the $C_{pCu}(T)$ of the Cu matrix and the $C_{pNb3Sn}(B,T)$ of the Nb_3Sn superconductor using the rule of mixture:

$$C_p(B,T) = \lambda \cdot C_{pNb_3Sn}(B,T) + (1-\lambda) \cdot C_{pCu}(T),$$

where λ is the volume fraction of superconductor. Specific heat data for copper and Nb_3Sn superconductor at various temperatures can be found, for example, in [20].

The *filament twist pitch l_p* controls the eddy currents in superconducting composite wires when subjected to varying magnetic fields, and hence the wire magnetization and AC losses. The typical value of twist pitch in superconducting composite wires is ~10·D, which is sufficient to suppress eddy current effects to an acceptable level.

The *Cu to non-Cu ratio* is an important parameter for composite wire stabilization and for magnet quench protection. It also plays a significant role in the processing of multifilament composite wires.

A high Cu/non-Cu ratio is required to limit the maximum temperature in the coil and the voltages in the magnet during quench. It also improves the wire stability with respect to the thermal perturbations in the coil. A low Cu/non-Cu ratio increases the fraction of superconductor in the coil and, thus, reduces the coil volume.

The *matrix axial resistivity ρ_m* determines the voltage and Joule heating power generated in a composite wire by the transport current during the superconductor transition from superconducting to normal state. The *transverse resistivity ρ_e* determines the level of eddy currents and thus eddy current magnetization and AC loss power in composite wires. These two parameters are related as follows [34]:

$$\rho_m \frac{1-\lambda}{1+\lambda} \le \rho_e \le \rho_m \frac{1+\lambda}{1-\lambda}$$

The *Residual Resistivity Ratio* (*RRR*), defined as the ratio of the Cu matrix resistivity at room temperature R_{300K} to its residual resistivity R_{Tc} at a temperature slightly above the superconductor critical temperature T_c=18 K, is a measure of Cu matrix purity, which is important for wire dynamic stabilization and magnet quench protection. Typical values of *RRR* for PIT and IT composite wires are of about 200. The *RRR* depends on the amount of Sn in the billet, on the diffusion barrier thickness and on the heat treatment cycle. A low *RRR* indicates damage of the internal structure of the wire and Sn leakage into the surrounding Cu stabilizer. The *RRR* is also subject to magneto-resistivity, i.e. its value decreases at increasing magnetic fields, and can be affected also by the cabling process.

The present *cost* of Nb_3Sn composite wires exceeds the cost of Nb-Ti wires by a factor of 5 to 10. A significant reduction of Nb_3Sn wire cost is required to make this technology fully attractive for large superconducting accelerators. Taking into account that the fabrication technology of Nb_3Sn wires is similar to that of Nb-Ti wires and that it does not use any rare or expensive components, it is believed that Nb_3Sn wire cost could be reduced by a factor of 2 to 3 from the present value. A sizable reduction of Nb_3Sn wire cost is also expected at large-scale production. A cost analysis of Nb_3Sn composite wires for high-field magnets can be found in [35].

D. Nb_3Sn Wire R&D Programs

In 1999 the U.S. Department of Energy has started the Conductor Development Program (CDP) [36] as a collaborative effort of U.S. industry, national laboratories and universities with the goal of increasing the critical current density of Nb_3Sn IT wires for HEP applications including high field accelerator magnets. The target Nb_3Sn strand parameters for the superconductor R&D efforts by CDP are summarized below:

- Non-copper J_c at 12 T and 4.2 K – 3000 A/mm^2
- Effective filament size – smaller than 40 μm
- Strand unit length – greater than 10 km
- Heat treatment time – less than 200 h
- Conductor cost – less than $1.50 kA-m at 12 T, 4.2 K

As a result of this program, multifilament Nb_3Sn composite wires produced using the Restacked Rod Process (RRP®) by OST, demonstrated critical current density J_c at 12 T and 4.2 K above 3 kA/mm^2 [10], [37], and Nb Rod-in-Cu Tube (RIT) wires by Outokumpu reached 2.7 kA/mm^2 [38]. In parallel the CDP was focused on the optimization of J_c, Cu matrix *RRR*, effective filament diameter d_{eff} and subelement spacing to develop wires for 10 to 12 T superconducting accelerator magnets stable with respect to flux jumps.

At the same time DOE funded Nb_3Sn strand design and technology development in the framework of the Small Business Innovation Research (SBIR) program [39]. The SBIR was focused on the IT and PIT wires, improving wire J_c, increasing stability and lowering wire magnetization and AC losses by reducing the d_{eff} (increase the number of subelements), etc.

A parallel R&D started in early 2000s in the European Union as part of the Next European Dipole (NED) program [19]. This effort was focused on the development of composite Nb_3Sn wires of large diameter (wire diameter up to 1.25 mm), with a J_c of 1.5 kA/mm^2 at 4.2 K and at the higher field of 15 T, produced by two methods: Enhanced Internal Tin (EIT) [24] and Powder in Tube (PIT) [40]. The target Nb_3Sn strand parameters for the NED superconductor R&D efforts are summarized below:

- Non-copper J_c at 15 T and 4.2 K – 1500 A/mm^2
- Effective filament size – smaller than 50 μm
- Wire diameter – 1.250 mm
- *RRR* – higher than 200
- Billet weight – 50 kg

At present this effort, led by CERN for the High Luminosity LHC (HL-LHC) upgrades, is concentrating on optimization of PIT wires at Bruker EAS.

The development of Nb_3Sn composite wires for accelerator magnets was also carried out on a smaller level in Japan at Mitsubishi Electric. This work focused on the combination of

high J_c, high *RRR* and small d_{eff} using the Distributed Tin (DT) method [23]. At present the Nb_3Sn wire R&D and production in Japan are carried out mainly by the National Institute for Materials Science, NIMS (bronze method), Furukawa (bronze method), JASTEC (bronze and DT methods) and SH Copper (bronze and DT methods) [41].

E. Commercial Nb_3Sn Wires

1) Internal Tin Wires

IT composite wires were produced by several companies. In the US it was done by IGC (Outokumpu since 2000, Luvata since 2005) and later by OST. OST has been producing IT Nb_3Sn using two basic approaches: single diffusion barrier and distributed diffusion barrier. The former has highly spaced filaments that don't touch after reaction, ideal to produce the low hysteresis losses required for ITER magnets, and the latter has densely packed filaments that touch after reaction to act as single subelement, and is used in applications where J_c is the most important property. Cross sections of wire designs produced by OST for accelerator magnets are shown in Fig. 3.

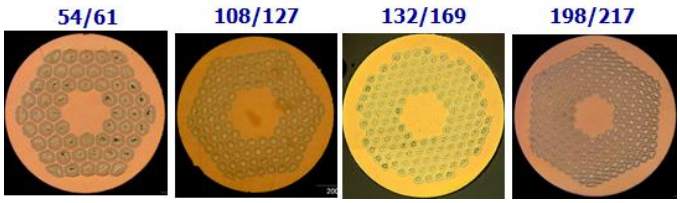

Fig. 3. Cross sections of RRP® wires designed at OST (courtesy of OST). The first number represent the number of SC subelements and the second number corresponds to the total number of restacks in the core.

Optimization of the IT strand design and of its processing, fostered by the US DOE Conductor Development Program (CDP), produced in the US a fast progress in $J_c(12T,4.2K)$ from ~1.5 kA/mm^2 to more than 3 kA/mm^2 from 1999 to 2006 (see Fig. 4). It was achieved first in a RRP® wire of 54/61 design 0.7 mm in diameter by OST [42]. The peak value of $J_c(12T,4.2K)$ in RRP® wire production at OST has been essentially stable over the past 10 years. An order of magnitude jump in production volume occurred in 2006 and then by a factor of 2 to 3 in 2012 and it continues growing. The minimal level of $J_c(12T,4.2K)$ in the commercial wires is above 2.5 kA/mm^2.

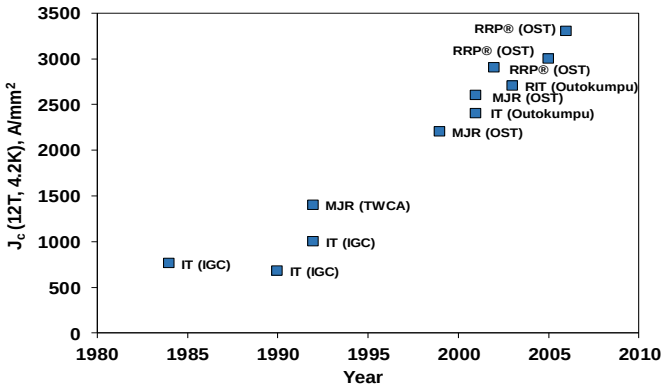

Fig. 4. $J_c(12T, 4.2K)$ as a function of time for IT Nb_3Sn composite wires. TWCA in Figure stands for Teledyne Wah Chang Albany.

Over the past ten years OST has produced several tons of high J_c RRP® wire of 54/61 configuration for HEP applications. RRP® is a distributed barrier IT strand having a Nb based diffusion barrier, therefore the subelement size d_{SE} is a good approximation for the d_{eff}. At 0.8 mm size this wire had a d_{SE} ~80 μm. When the impact of d_{eff} on magnet stability at low field became fully apparent in the accelerator magnet community, OST focused on increasing stack count in a billet while maintaining at the same time volume scalable processes. To reduce subelement merging during cabling, the Cu spacing between subelements was also increased. A second generation strand with 127 stack design entered production in 2008, with several tons utilized in HEP at 0.7 to 0.8 mm diameter and d_{SE} of 45 to 52 μm. A third generation wire with 169 stack design followed in 2011 [43]. This wire has d_{SE} of 40 to 58 μm for sizes of 0.7 to 1 mm. Integrated volume production of 169 stack RRP® billets at OST is approaching that of the 127 stack billets. The 217 stack wire is still in the R&D phase.

A couple years ago OST switched from using Ta-doped Nb filaments to interspersing Ti rods among the Nb filaments. This allowed lowering the wire optimal reaction temperatures to ~665°C with respect to the Ta-doped wire (~695°C) [43], thereby increasing the wire J_c at high fields, better preserving *RRR*, and improving the irreversible strain limit [44].

To maintain good *RRR*, OST has also been working on optimizing the Sn fraction in the billet, as well as the diffusion barrier thickness [43]. With the present subelement design, holding *RRR*>100 as d_{SE} decreases below ~45 μm results in lower J_c. This is caused by the need to under-react to preserve *RRR*, the need for higher Nb:Sn ratios, and smaller Sn diffusion channels.

2) Powder-in-Tube Wires

The PIT process was first developed by the Netherlands Energy Research Foundation (ECN) and further optimized by the Shape Metal Innovation Company (SMI) [12]. In 2006 Bruker EAS in Germany purchased the 'know-how' of the PIT technology to industrialize this type of conductor. Some PIT composite wires produced by SMI and now by Bruker EAS are shown in Fig. 5.

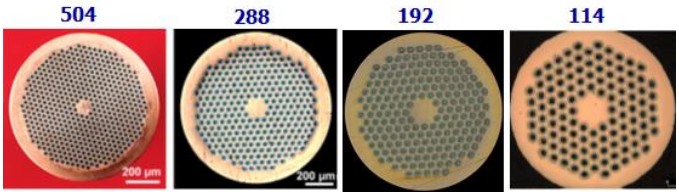

Fig. 5. Cross sections of PIT wires of different designs (courtesy of SMI and Bruker EAS).

The J_c as a function of time for $NbSn_2$ powder based PIT processed wires is shown in Fig. 6. The development of this technique has allowed producing km-long wires with 192 filaments. Shorter laboratory-scale wire samples with 1332 filaments were also obtained [15]. This method could allow an optimal combination of small filament size (<50 μm) and high J_c comparable to the IT process. Wires are presently manufactured at Bruker EAS in about 50 kg net production units. The maximum non-Cu J_c has reached ~2.7 kA/mm^2 at

12 T and 4.2 K in 1.25 mm wires with 288 filaments of 50 μm, developed for the Next European Dipole (NED) program. For commercial PIT wire production at Bruker EAS, the $J_c(12T,4.2K)$ is between 2.4 and 2.5 kA/mm^2, and the wire *RRR* is typically between 100 and 200. The PIT wire design was recently optimized at Bruker EAS by using round filaments to keep both J_c and *RRR* high during HT. Wire production yield is very good.

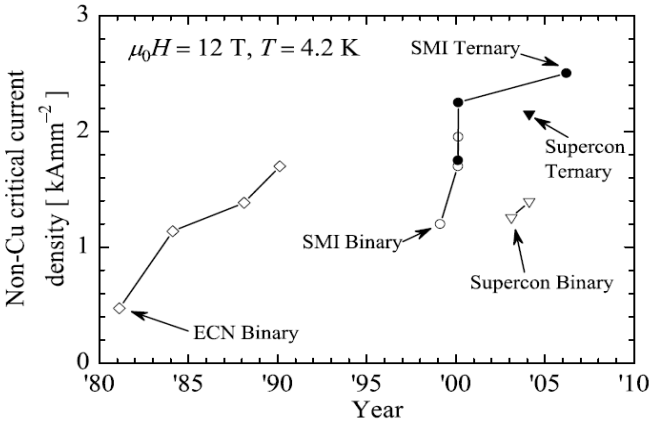

Fig. 6. Non-Cu J_c as a function of time for binary and ternary $NbSn_2$ powder based PIT processed wires [11].

The RRP® 108/127 design shown in Fig. 3 and PIT layouts with 114 and 192 filaments shown in Fig. 5 are being considered for use in Nb_3Sn 11 T dipoles and 150-mm aperture quadrupoles developed for LHC upgrades [45].

3) SBIR programs

Nb_3Sn wires for accelerator magnet applications are also being developed and produced in the U.S. at Supercon Shrewsbury (MA), SupraMagnetics (CT), Supergenics (MA) and Hyper Tech (OH). The R&D work on these wire was partially funded by the US DOE SBIR program.

Supercon had produced multifilament Nb_3Sn wire by the PIT approach with filament diameter below 60 μm in the past [46]. Multifilament Nb_3Sn superconductor was also produced at Supercon by the Internal Tin Tube (ITT) approach [47], using tubular Nb filaments with Sn or high-Sn alloy cores inside a copper sheath. Non-Cu J_c values of 1.8 kA/mm^2 at 12 T and 4.2 K were achieved in this layout.

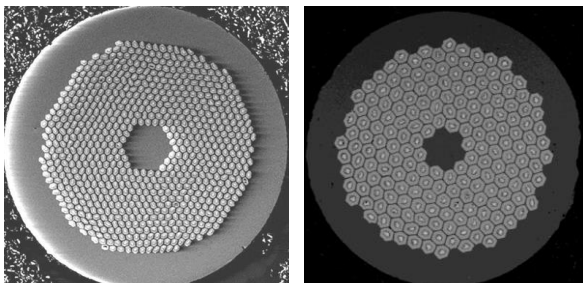

Fig. 7. 0.7 mm diameter wires with 744 Nb_3Sn filaments (left) and with 192 Nb_3Sn filaments (right) (courtesy of Hyper Tech).

Hyper Tech (Columbus, OH) had developed in collaboration with Supergenics [48]-[50] and has been manufacturing a tube type Nb_3Sn wire by using pure Sn and Sn-alloy cores as a Sn source. Samples from wires with 744 filaments of 18 μm size carried a maximum non-Cu J_c at 12 T and 4.2 K of ~2.1 kA/mm^2. Samples with 192 filaments of 35 μm size ~2.5 kA/mm^2. The cross section of both wires are shown in Fig. 7. For the 0.7 mm diameter wire with 192 filaments, piece lengths of more than 3 km have been achieved without breakage. Progress still has to be realized to make these wires sufficiently resistant to the cabling process.

Recently Hyper Tech, in collaboration with Ohio State University (Columbus, OH), demonstrated that SnO_2 in tubular Nb_3Sn strands could be used to form ZrO_2 for pinning and refine the Nb_3Sn A15 grain size from 100 nm to 40 to 50 nm, which increases the layer J_c up to 10 kA/mm^2 at 12 T and 4.2 K [51]. This is about a factor of 2 higher than regular Nb_3Sn strands. This discovery opens up the potential of 16 to 20 T accelerator magnets if these finer grain size wires can be fully developed.

SupraMagnetics [52], [53] has been making PIT wires with jet-milled Cu_5Sn_4 powder. This approach has several advantages: a) it provides a Sn source without using the more expensive $NbSn_2$ powder; b) Cu is already an integral part of the intermetallic and it does not need to be added separately as in the case of $NbSn_2$ PIT process, which uses a Cu tube; and c) processing of the Cu_5Sn_4 is simpler and less expensive. Monel and Glid Cop Al-15 are used to internally strengthen the wires as a whole via a novel octagonal design of the subelements. Best non-Cu J_c value for this PIT approach was 2.5 kA/mm^2 at 12 T and 4.2 K.

SupraMagnetics is also working on incorporation of ZrO_2 precipitates via the approach introduced in [51]. Similar results have been achieved by the PIT process in a multifilament wire by mixing SnO_2 powder into the Cu_5Sn_4 jet-milled powder. During HT the oxygen diffuses into the Nb-1%Zr tube, forming ZrO_2 precipitates which slow grain growth to only 40 to 50 nm. Magnetic measurement have shown a shift toward point-like pinning in the pinning strength. Without the ZrO_2 the pinning follows a classic Kramer grain boundary-like pinning in the PIT wires. The company is also working on a new Nb_3Sn process with a novel Artificial Pinning Center (APC) for HEP and High Magnetic Field Applications.

III. Nb_3Sn Wire Properties

In this section, we detail those key research activities and methods used in the international community that helped study and solve most of the aspects required of Nb_3Sn wires for accelerator magnet realization. This includes I_c and J_c improvements, *RRR* effects, strain sensitivity, magnetization and stability to flux jumps.

A. I_c, J_c Improvement

Whereas both T_{co} and B_{c20} depend on the material chemical composition, J_c rests also on the superconductor microstructure, which controls the flux pinning mechanisms. In particular, in 1966 it was shown [54] that J_c in Nb_3Sn thin tapes obtained by chemical vapor deposition is inversely proportional to grain size. In 1976, the J_c decrease for smaller grain sizes, after going through a maximum, was also calculated [55]. Earlier [54] and later experiments in multifilamentary bronze wires [56], [57] corroborated that the

J_c decreased for grain sizes below ~40 to 80 nm. More recently, Nb_3Sn thin films obtained by e-beam coevaporation and subsequent heat treatment showed the best properties at 20 to 25 nm of grain size [58]. The physical limit occurs for grain sizes smaller than the vortex spacing.

1) Flux Pinning Models

Nb-Ti and Nb_3Sn feature very different J_c scaling behavior with respect to magnetic flux density and temperature [20], [29]-[32], [59]-[63]. Experimental studies [59], [61], [64], [65] have found that A15 superconductors, such as Nb_3Sn, consist mainly of radial and equiaxed superconducting grains separated by ~2 nm thick layers. The elongated, axial structure of cell walls in Nb-Ti seems to lead exclusively to 'transverse pinning', while the equiaxed grain structure of Nb_3Sn tends to lead to 'longitudinal pinning' behavior over most of the field regime [59]. This difference has been attributed to different mechanisms of flux motion [59], [60], [62]: the scaling behavior of Nb-Ti has been associated with pin breaking, while that of Nb_3Sn has been identified with flux shearing. For instance, Kramer's model is based on flux shear. However, this model used questionable assumptions (for instance a high field limit for the shear modulus), required unrealistic physics parameters, most notably it did not contain the observed grain-size dependence of J_c, and employed an expression for the shear modulus valid only at high fields. These various deficiencies have left the physical picture somewhat incomplete [59] and since then, a number of additional attempts were made to explain the observed $J_c(B,T)$ by either flux shearing or pin breaking.

Many of the observed features of the magnetic and transport properties of Nb_3Sn, as well as of other A15 materials, could be understood by modeling them as a collection of strongly coupled superconducting grains and taking into account the anisotropic flux pinning by grain boundaries [66]. Because of the strong coupling of the grains, the junctions were treated within the framework of nonlocal Josephson electrodynamics (NLJE). Each junction was described by a maximum Josephson current density J_0, above which the gauge-invariant phase difference across the junction, $\Delta\gamma$, starts to slip leading to a voltage drop. In this model, J_c is determined solely by grain boundary pinning. Nevertheless, this single mechanism leads to two different scaling laws because of the anisotropy of the pinning forces. This approach led to the observed scaling behavior of Nb_3Sn over a majority of the field range, provided a clear physical picture of its origin by reproducing many of the features seen experimentally, as well as a plausible explanation for the deviations at low and high fields and at high temperatures.

2) IT Composite Wires

The J_c of IT Nb_3Sn is affected by design parameters such as subelement size, number of restacks, relative amount of Sn and Nb in the non-Cu section, and type of ternary material in the Nb_3Sn. To reach high J_c values, both the quantity (the amount of superconductor that is formed in the non-Cu fraction) and the quality (grain refinement, Sn content, and ternary element addition) of the Nb_3Sn must be optimized. This is possible by reducing the fraction of Cu in the matrix to a practical manufacturing minimum in the range of 0.1 to 0.3, by introducing alloying additions such as Ta or Ti, and by an optimized HT schedule. When the barrier that separates the multifilamentary regions from the high-purity Cu is made of Nb, it is partially reacted during heat treatment, thus adding to the final superconducting cross section. After HT, the tightly packed Nb filaments and the reacted portion of the barrier grow into a completely connected volume of Nb_3Sn, fully coupled, and whose typical dimension is approximately the size of the stacked subelement.

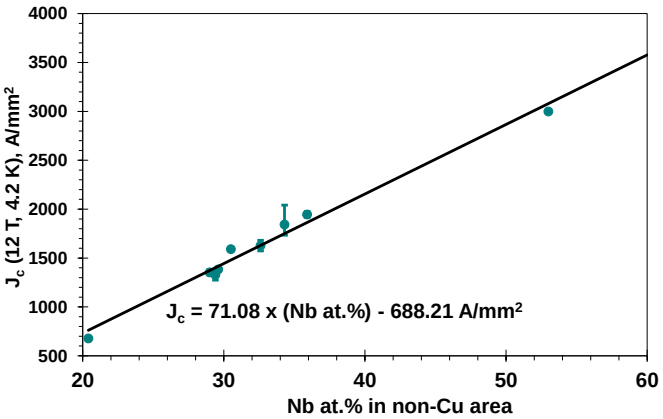

Fig. 8. $J_c(12T,4.2K)$ values plotted against Nb content in the wire as produced by different IT strands having undergone similar HT cycles.

As well-known by wire manufacturers, the J_c of IT strands is proportional to the Nb content in the non-Cu area of a wire. The example in [67] reported $J_c(12T,4.2K)$ values over the non-Cu area against Nb at.% in the non-Cu section of different IT wires having undergone similar HT cycles (Fig. 8). Because of the linear behavior, it was predicted at the time that to reach a $J_c(12T,4.2K)$ of 3000 A/mm^2 would have required about 50at.% Nb when using the IT technology. This was later confirmed when Nb_3Sn OST wires achieved such high J_c's [68] (Fig. 8). The physical limit imposed by stoichiometry implies a maximum theoretical non-Cu $J_c(12T,4.2K)$ of ~5000 A/mm^2 by extrapolation to 75at.% Nb in the non-Cu area.

A larger number of subelements in the strand appeared to increase heat treatment efficiency in forming the Nb_3Sn A15 phase. This was inferred by the different times needed by 19 subelement designs with respect to 37 or 61 subelement designs to reach the peak J_c. Whereas the former required 50 to 70 h, the latter needed only 40 to 50 h [69].

3) PIT Composite Wires

The J_c of PIT Nb_3Sn is affected by design parameters such as filament size, number of Nb tubes, use of binary Nb_3Sn or ternary $(NbTa)_3Sn$, and quality and size of the $NbSn_2$ powder.

An interesting experiment showed for instance how to optimize filament size for J_c in PIT wires [70]. This can be done by measuring the superconducting layer thickness and associated layer J_c as function of reaction time and temperature. Since at a given reaction temperature the layer J_c appears to peak with time and then decrease, the corresponding size of the superconducting layer formed at the temperature that produced the maximum J_c is a good

indication of filament thickness required in the wire design. Fig. 9 shows this method for 1 mm PIT wires with 192 tubes of ~50 μm outer diameter and thickness of 12 to 13 μm. The layer J_c peaked at a reaction temperature of 700°C, at which a superconducting layer formed of ~ 10 to 11 μm. This wire was well-designed as it allowed for 2 to 3 μm of outer unreacted Nb in the tubes in order to preserve *RRR*.

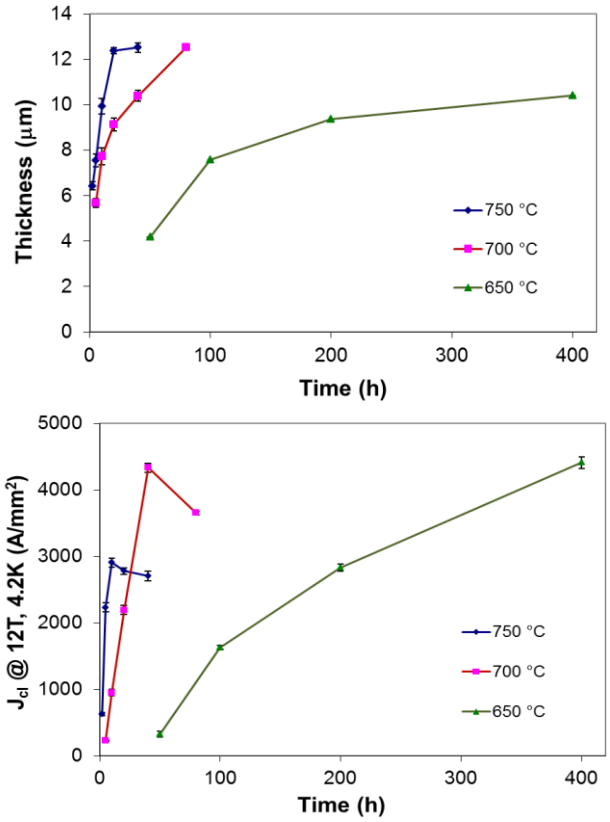

Fig. 9. Nb_3Sn layer growth (top) and layer J_c at 12 T and 4.2 K (bottom) vs. HT time and temperature for a 1 mm PIT wire with ~50 μm Nb tubes [70].

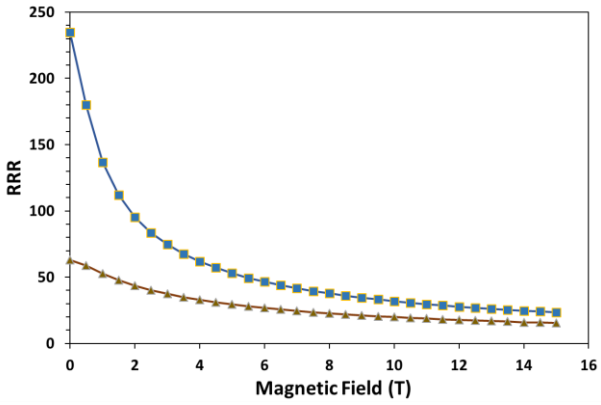

Fig. 10. *RRR* vs. *B* measured for two different 0.7 mm RRP® round wires with *RRR* values of 235 and 60 (courtesy of D. Turrioni, FNAL).

B. RRR

Typical *RRR* values for present PIT and IT round wires are of about 200. A low *RRR* indicates damage of the wire internal structure and Sn leakage into the surrounding Cu stabilizer. For IT, the *RRR* depends strongly on the amount of Sn in the billet and on the Nb barrier thickness, ranging from about 20, to 60, to 160 for barrier thicknesses of 3, 4.2 and 6 μm respectively. For both PIT and IT wires the *RRR* depends on the heat treatment cycle [71].

The *RRR* of round wires reduces due to the magneto-resistivity effect (see Fig. 10), i.e. its value strongly decreases with increasing magnetic field. This effect is stronger for a higher purity Cu matrix, thereby reducing the importance of high *RRR* at larger fields.

C. Stress/strain Sensitivity

The A15 cubic crystal structure is modified by strain into a tetragonal phase, which causes a reduction of the intrinsic superconducting properties of the compound. The produced distortions, whose energy is on the scale of the mRydberg, move the Fermi energy E_F to higher values with respect to the undeformed cubic phase. It is known that such variations are correlated to strain-induced modifications in both the phononic and electronic properties. The strain-induced modifications in the average phonon frequencies and in the bare electronic density of states $N(E_F)$ at the Fermi energy contribute to strain-induced degradation of T_c in Nb_3Sn [72]. It was recently shown from data analysis of Nb_3Sn samples that $N(E_F)$ decreased by 15 to 30% as T_c varied from 17.4 to 16.6 K under external axial strain, and that the relationship between $N(E_F)$ and T_c in strained Nb_3Sn strands shows significant difference between tensile and compressive loads [73]. Because higher magnetic fields produce proportionally higher Lorentz forces, 3D strain sensitivity of critical current is a very important property in superconductors. In addition, Nb_3Sn is brittle. In bulk form it fractures at a tensile strain of ~ 0.3%. In a multi-filamentary composite wire, where the Nb_3Sn filaments are supported by a surrounding Cu matrix, it can be strained to ~ 0.7% before fracture.

1) Tensile/compressive Strain Degradation

The strain behavior for a number of Nb_3Sn RRP® wires is shown in Fig. 11 [74], which presents the normalized $I_c(4.2K,15T)$ vs. axial intrinsic strain. The irreversible strain can be also identified. The irreversible intrinsic strain of Ta-doped Nb_3Sn wires is less than +0.11%, to be compared with the irreversible intrinsic strain range of +0.26% to +0.31% found for Ti-doped wires, consistently with NIST studies [44].

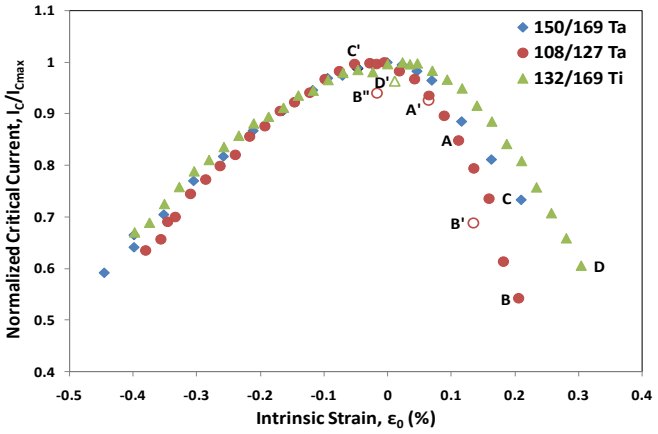

Fig. 11. Normalized $I_c(15T,4.2K)$ vs. longitudinal intrinsic strain for 0.7 mm samples of Ta-alloyed 108/127 RRP®, Ta-alloyed 150/169 RRP® and Ti-doped 132/169 RRP® wires [74].

2) Bending Degradation

The I_c degradation of Nb_3Sn wires due to bending is important when using the React&Wind technique as opposed to the Wind&React approach. In the former a magnet is wound with an unreacted cable, in the latter the cable is reacted on a spool of given diameter before being used for winding the coils. Bending degradation was measured in [75], by reacting Nb_3Sn wire samples on smaller sample holders than those used for I_c measurements. The results of I_c measurements made on unbent strands were compared with those made on IT and MJR wires with a maximum bending strain of about 0.2% and 0.4%. Based on these data, for React&Wind magnets that featured a minimum bending radius of 90 mm (*i.e.* maximum bending strain of about 0.2% for a 0.7 mm wire), the bending degradation at 12T was expected to be less than 7% for the MJR material and less than 5% for the IT material [76].

Bending degradation was also measured on cables made of the same IT wire as above. The cables were reacted while bent on a 290 mm diameter reaction spool, and straightened before impregnation and measurement. Results were compared with those of unbent samples. An excellent correlation between strand and cable tests was found for cables without a resistive core, whose strand layers bent independently [77].

D. Wire Magnetization

Magnetization loops measured at low field ramp rates (dB/dt<0.02 T/s) between 0 and 3 T for IT (MJR and RRP®) and PIT wires are shown in Fig. 12 per non-Cu volume. The eddy current component of magnetization in Nb_3Sn composite wires is suppressed by using a small wire twist pitch. For l_p<15 mm and a rather low ρ_e~10^{-10} Ω·m, the eddy current magnetization component is less that 1% of the hysteretic component at dB/dt<0.1 T/s, which are typical maximum field variation rates in accelerator magnets.

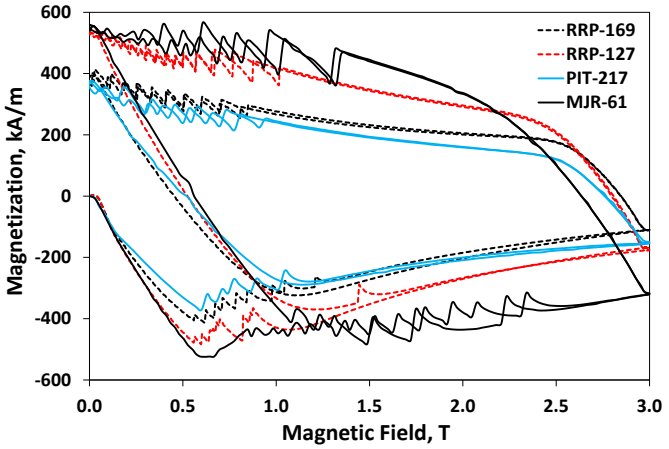

Fig. 12. Magnetization curves per non-Cu volume: a) MJR-61 1 mm, d_{eff}~100 µm, $J_c(12T,4.2K)$~2.0 kA/mm^2; b) PIT-217 1 mm, d_{eff}~50 µm, $J_c(12T,4.2K)$~2.1 kA/mm^2; c) RRP-127 0.7 mm, d_{eff}~45 µm, $J_c(12T,4.2K)$~2.9 kA/mm^2; d) RRP-169 0.7 mm, d_{eff}~40 µm, $J_c(12T,4.2K)$~2.7 kA/mm^2.

As expected for the hysteretic component, the magnetization loop width is larger for wires with higher J_c and larger d_{eff}. Due to the larger J_c and d_{eff}, the level of wire magnetization as well as the range of wire re-magnetization when dB/dt changes sign are more than an order of magnitude larger than for Nb-Ti wires used in accelerator magnets. The large level of magnetization and associated flux jumps lead to field quality deterioration. Flux jumps also produce some field uncertainties in accelerator magnets at low fields from cycle to cycle [78].

E. Flux Jumps

Flux jumps in Nb_3Sn composite wires, predicted by stability criteria (see section II.C) at fields below certain levels [20], [79], are observed in magnetization [80]-[83] and critical current measurements [71], [84]-[86]. Flux jumps in magnetization measurements are seen for instance in Fig. 12. In critical current measurements the flux jumps are recorded as large voltage spikes and premature quenches below the superconductor critical surface $I_c(B,T)$ during either current ramping in a fixed magnetic field (*V–I* measurements) or field ramping at a fixed transport current (*V–H* measurements). An example of flux jump instabilities in critical current measurements is shown in Fig. 13.

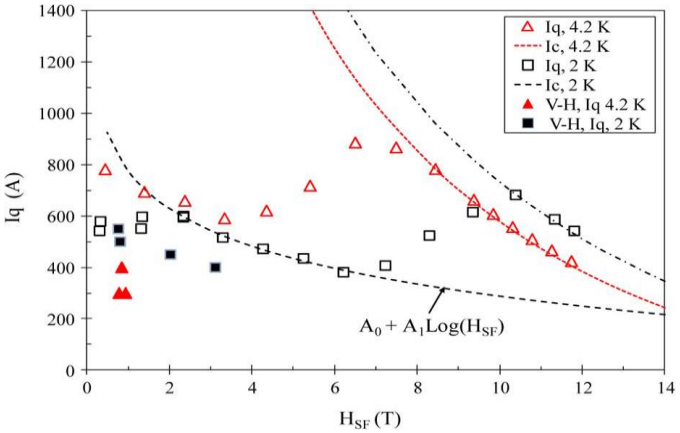

Fig. 13. *V-I* measurements of a Nb_3Sn wire critical current at 4.2 K and 2 K. *V-H* results are shown by solid markers [87].

Some authors distinguish two types of flux jump instabilities – 'magnetization' and 'self-field' instabilities. Note that the magnetic flux profile in a composite wire is a superposition of the magnetic flux from persistent (or magnetization) currents and the magnetic flux from transport current. Pure so-called 'magnetization' instabilities occur in magnetization measurements without a transport current, whereas pure 'self-field' instabilities occur during critical current measurements at zero external field or in the vicinity of the critical surface. In reality, instabilities are usually observed in the presence of both an external field and a transport current, and therefore are a combination of these two cases. As can be seen from Fig. 13, superconducting wires can carry some transport current even in the presence of flux jumps. This was first recognized and shown theoretically by R. Hancox [88] in the 1960s using the enthalpy stabilization approach and partial flux jump concept. Theoretical and experimental studies of electromagnetic instabilities in modern Nb_3Sn strands are reported elsewhere [89]-[93].

An example of calculations of strand maximum transport current $I_t(B)$ in an external magnetic field for Nb_3Sn wires is

shown in Fig. 14 in the case of uniform current distribution in the wire cross section [78]. Similar calculations for non-uniform distribution of a transport current are presented in [91]. These calculations predict significant reduction of wire current carrying capability at low fields with respect to its critical current $I_c(B)$ for Nb_3Sn high-J_c composite wires presently used in accelerator magnets. Furthermore, for wires with large d_{eff} and high J_c, the maximum transport current (or transport current density) at low fields can be smaller than the transport current at high fields (see Fig. 14). Premature quenches in magnets may occur if the load lines of a magnet encompass an instability region in the conductor $I(B)$ curve (case A in Fig. 14). To determine the minimum in the $I(B)$ curve requires to perform V-I and V-H strand measurements in the whole range of magnetic fields. The instability current, I_S, is typically defined as the minimum quench current obtained in the V-H test.

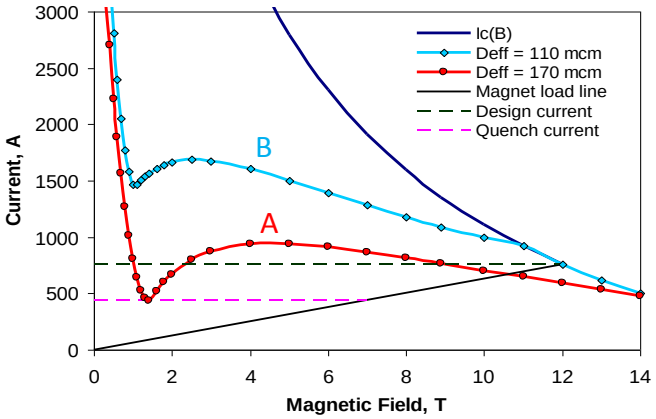

Fig. 14. Calculated maximum current in Nb_3Sn wires vs. field and maximum field for a magnet with flux jumps in conductor [78].

In [94], when analyzing the effect of subelement size and *RRR* on the instability current density J_S, it was possible to identify just two sets of RRP® round wires with *RRR* values larger and smaller than 60 to find a common behavior of J_S with d_{eff}. This is apparent in Fig. 15, where the J_S at 4.2 K dependence on subelement size is shown for RRP® round wires of 0.5 to 1 mm diameter, and higher and lower *RRRs*.

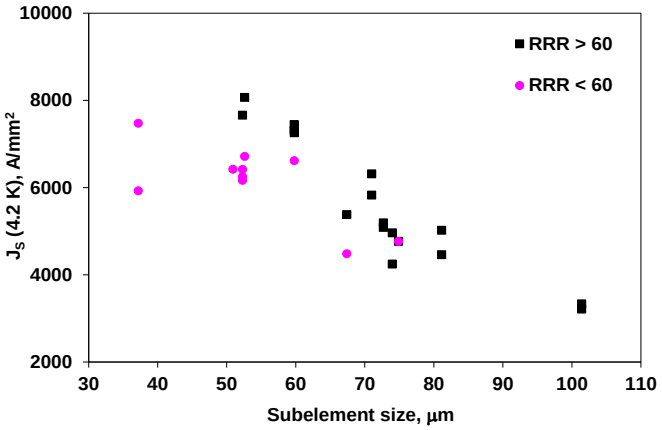

Fig. 15. J_S at 4.2K vs. subelement size for RRP® round wires of 0.5 to 1 mm diameter. The samples in the *RRR*<60 set had *RRR* values down to 11 and $J_c(12T,4.2K)$ between 2.45 and 2.92 kA/mm^2. The samples in the *RRR*>60 set had *RRR* values up to 300 and $J_c(12T,4.2K)$ between 2.38 and 3.13 kA/mm^2.

In Fig. 16, data from BNL, FNAL and LBNL are shown as $J_S(B)$ normalized to the expected $J_c(B)$. Flux jumps clearly reduce superconductor current to only 5 to 20% of the critical surface in the shown *RRR* range.

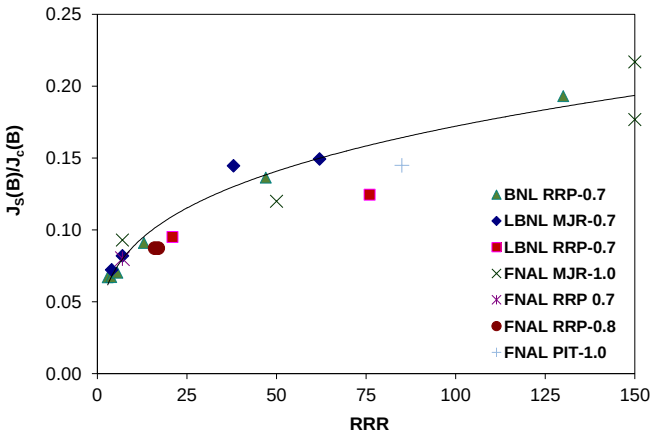

Fig. 16. Effect of *RRR* on J_c degradation due to flux jumps at low fields.

A parametric study was performed by using Finite Element Modeling on strands [93] to quantify the effect of *RRR* on stability. The quench current at 4.3 K was computed for the minimum in the low field region and for 12 T in the case of 'self-field' instability and large perturbations. According to this study, high-field instability does not improve much by increasing the *RRR* above 100 (partially due to the magneto-resistance effect dominating the electrical and thermal conductivity properties of the copper at high magnetic fields).

Flux jumps in Nb_3Sn composite wires manifest themselves also as distinct voltage spikes in voltage-current and voltage-field measurements [95]. Their origin is related to magnetization flux jump and transport current redistribution, respectively. The large amplitude and high intensity of these spikes at low field can cause premature trips of the magnet quench detection system, due to large voltage transients or quenches at low current [96].

IV. Nb_3Sn Rutherford Cables

Three-side views and cross sections of a 40-strand Nb_3Sn Rutherford cable with keystoned geometry are shown in Fig. 17 [97].

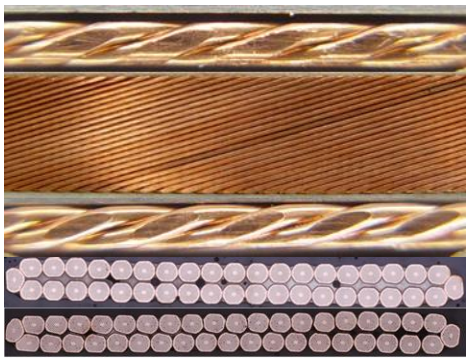

Fig. 17. Three-side views of a Nb_3Sn Rutherford cable with a keystoned cross section (top), cable rectangular (middle) and keystoned (bottom) cross sections [97].

In this section, we identify fundamental electromagnetic and geometric parameters of Nb_3Sn cables, including the effects from cabling on the strands and their subelements, briefly touch on quality control and summarize findings on cable volume change during heat treatment.

A. Electromagnetic Parameters

The maximum value of a cable critical current I_c is the sum of the strands critical currents I_{ci}. The actual total current I_c is somewhat lower, due to the degradation of strand performance during cabling g_i:

$$I_c = \sum_{i=0}^{N} g_i I_{ci} \,,$$

where N is the number of strands in a cable.

Due to electromagnetic coupling between strands, the Rutherford cable magnetization and AC losses components include additional eddy current contributions controlled by the cable geometry and interstrand contact resistance [98]-[100]. The additional cable magnetization and loss power, caused by the inter-strand eddy currents in the cable, are determined by the following formulas:

$$\vec{M}_c = -\mu_0 \cdot \left(\frac{8}{15}\frac{\alpha^2 L^2}{\rho_c}\frac{d\vec{B}_\perp}{dt} + \frac{1}{3}\frac{L^2}{\rho_a}\frac{d\vec{B}_\perp}{dt} + \frac{1}{4}\frac{L^2}{\alpha^2\rho_a}\frac{d\vec{B}_{||}}{dt}\right),$$

$$P_c = \frac{8}{15}\frac{\alpha^2 L^2 \dot{B}_\perp^2}{\rho_c} + \frac{1}{3}\frac{L^2 \dot{B}_\perp^2}{\rho_a} + \frac{1}{4}\frac{L^2 \dot{B}_{||}^2}{\alpha^2 \rho_a},$$

where $4L$ is the cable transposition pitch, α is the cable aspect ratio (the ratio of the cable width w to its mean thickness t), $B_\perp$ and $B_{||}$ are the perpendicular and parallel components of the magnetic field to the cable wide surface, and ρ_c and ρ_a are the effective cable resistivity between cable layers and within a layer respectively. The first term in both formulas provides the main contribution owing to the large value of α. The parameter ρ_c and the measurable value of the associated interstrand contact resistance R_c [101] are related as follows:

$$\rho_c = \frac{4\alpha L}{N^2} R_c.$$

To control eddy current magnetization and losses in a Rutherford cable, it is necessary to increase the contact resistance. This can be done in Nb_3Sn cables by coating strands with metal, e.g. Cr, which survives a high-temperature heat treatment. However, good current sharing between strands requires low contact resistances. The optimal way of reducing eddy current effects in a Rutherford cable without worsening current sharing is to increase R_c while keeping the adjacent contact resistance R_a low. This is done by using a thin resistive core inside the cable [99], typically of stainless steel.

The most important parameters, which define the performance of a Rutherford cable in a magnet, include critical current I_c and average critical current density J_A, Cu/non-Cu ratio, cable axial normal resistivity ρ_n and Residual Resistivity Ratio *RRR*, and interstrand resistances R_c and R_a. As in the case of single Nb_3Sn composite wires, the parameters of the HT cycle, which affect I_c, *RRR* and contact resistances R_c and R_a, as well as cable cost, are also very important.

B. Cable Design Parameters

The Rutherford cable geometry is characterized by a cable aspect ratio α and a cross section area S_{cbl}, determined by its width w, mid thickness t and keystone angle φ, cable pitch angle θ, and cable packing factor *PF*.

Pitch or transposition angle θ. The cable pitch angle affects the cable mechanical stability and the critical current degradation. Typical values of pitch angle in NbTi cables used in accelerator magnets were within 13 to 17 degree. A special study of the possible pitch angle range for Rutherford cables was performed using 1 mm hard Cu strand and 28-strand cable design, and 27 and 39 strand cables with 0.7 mm Cu Alloy68 strand [102]. It was found that for 1 mm strands, below 12 degree the cable shows mechanical instability and that at 16 degree and over, popped strands, sharp edges and crossovers start occurring. In the case of 0.7 mm strands, the stable range of transposition angles was within 9 to 16 degrees.

Cable packing factor PF. The cable packing factor, *PF*, is defined as the ratio of the total cross section of the strands to the cable cross section envelope $S_{cbl} = w{\cdot}t$:

$$PF \cong \frac{\pi N \cdot D^2}{4(w \cdot t - A_{core}) \cdot \cos\theta},$$

where N is the number of strands in the cable, D is the strand diameter, w and t are the average cable width and thickness, θ is the cable transposition angle, and A_{core} the cross section area of the core.

The minimal *PF* for a Rutherford cable, i.e. one having a non-deformed cross section, has a value of $\sim\pi/4=0.785$. To provide cable mechanical stability and precise width and thickness (parameters that are important for accelerator magnet coils), Rutherford cables are usually compacted by squeezing their cross section in both transverse directions. For an I_c degradation limited to 5 to 10%, increasing the cable *PF* allows raising also the cable average current density J_A, which is defined as follows:

$$J_A = I_c / S_{cbl}\,.$$

Cable edge and width deformation R_e, R_W. The critical current degradation is determined mainly by the amount of cable cross section deformation. The deformations of cable edge R_e and width R_w are defined as follows:

$$R_e = \frac{t}{2D}, \qquad R_w \cong \frac{2w \cdot \cos\theta}{N \cdot D},$$

where D is the strand diameter, N is the number of strands in the cable ($N=N+1$ in the case of odd N), and θ is the cable transposition angle.

Nb-Ti cables, which were used in the Tevatron, HERA, RHIC, UNK, SSC, and LHC, had a relatively large small edge deformation R_e~0.76 to 0.82. It was also experimentally established that the deformation of the cable width should be kept small, R_w~0.97 to 1.0. The *PF* of Nb-Ti cables was quite high, typically within 88 to 93%. Nb-Ti cables with cross section deformation in the above ranges have an I_c degradation of less than 5%. An additional important limitation on cable *PF* is related to cable sharp edges observed in cables with high *PF*s.

Large strand plastic deformations, which were acceptable for a ductile superconductor like Nb-Ti, are not suitable for the more delicate Nb_3Sn strand structure. An example of strand cross section, as deformed after cabling, is shown in Fig. 18 (left) [78]. Fig. 18 (right) shows the local subelement deformations due to barrier breakage and merging observed in some RRP® Nb_3Sn strands.

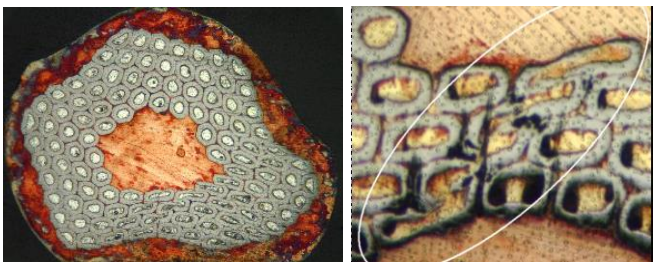

Fig. 18. Examples of deformed strand in a cable (left), and local subelement damage and merging (right) [78].

It has been found that the small edge deformation R_e in Nb_3Sn cables should be 0.85 or higher, and that the width deformation R_w should be slightly larger than 1.0, typically R_w=1.0 to 1.03, to avoid excessive strand deformation at the cable thin edge. The limits on small edge deformation and cable width define a value for the optimal keystone angle of the cable cross section. The nominal cable *PF* for Nb_3Sn cables is within 84 to 87%. This parameter space allows keeping the critical current degradation of Nb_3Sn Rutherford cables below 5 to 10%, and provides sufficient cable compaction to achieve adequate mechanical stability for coil winding, as well as high average critical density J_A.

Strand plastic deformation. By defining strand deformation ε_{str} as follows:

$$\varepsilon_{str} = \frac{d_{max} - d_{min}}{d_0},$$

where d_{max} and d_{min} are the longest and shortest diameters measured through the strand center, and d_0 is the original round strand size, a correlation could be found between the average deformation of all strands in a cable and its packing factor. This can be seen in Fig. 19 for a large statistical cable sample [103].

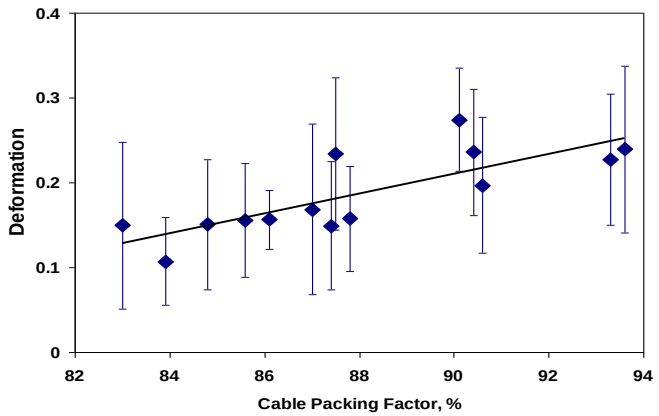

Fig. 19. Average strand deformation vs. cable *PF* for a large number of cables. Error bars represent the standard deviation of the deformation distribution [103].

Fig. 20 (bottom), where the deformation of each strand in a keystoned and rectangular cable is plotted as function of its position in the cable [102], [103], shows what happens locally in each strand. A schematic of strand location is in Fig. 20 (top). In both cables the largest deformation values are found in the strands at both cable edges. The average strand deformation is lower in the least compacted cable.

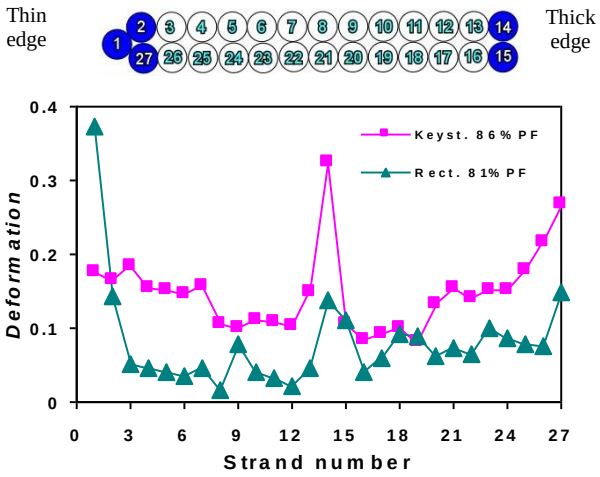

Fig. 20. Strand deformation as a function of position in 27-strand cable (bottom). A schematic of the strand locations is shown at the top [103].

Subelement plastic deformation. Similarly to the empirical formula used for strand deformation ε_{str}, subelement plastic deformation ε_{SE} could be defined as follows:

$$\varepsilon_{SE} = \frac{d_{max} - d_{min}}{d_0},$$

where d_{max} and d_{min} are the longest and shortest diameters measured through the subelement center, and d_0 is the original round subelement size.

Fig. 21 shows measured distributions of subelement d_{max} in round wires and in wires extracted from cables with different *PF*s.

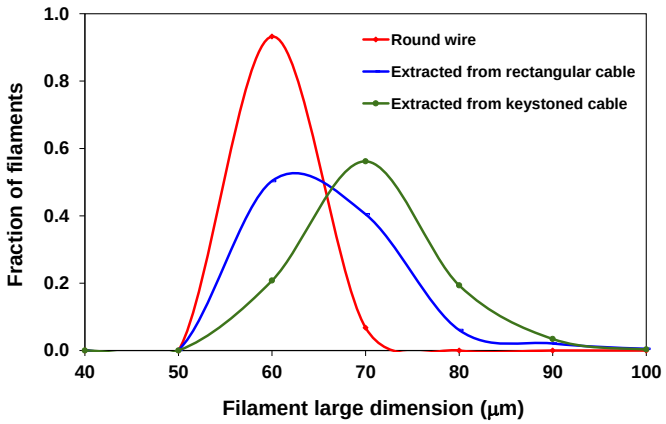

Fig. 21. Distributions of subelement largest dimension in round wire and in strands extracted from rectangular and keystoned cables with *PF*=88.6%.

The effects of cable width deformation on subelement plastic deformation were simulated using a Finite Element Model [104]-[110] for RRP® and PIT strands. These

simulations show that in a cable the largest values of plastic subelement deformation are generally located in the innermost part of the edge strand. These maximum values are plotted in Fig. 22 as function of width deformation R_w. A conclusion from these studies was that exceedingly compacting the cable in width produces a rapid increase in strain in the innermost part of the edge strand. Based on the simulations, the optimal value for width compaction R_w corresponds to zero plastic deformation in Fig. 22 and is 1.03 to 1.04.

In [14] the cable design width is described by the following empirical formula (N>10):

$$w=N\cdot D/(2\cos\theta) +0.72\cdot D\ ,$$

where N is the number of strands in a cable, D is the strand diameter, and θ is the cable pitch angle. It is to be noted that this formula gives R_w close to 1.04 only for N>35. For N<25, R_w is noticeably greater than 1.04, which could lead to mechanically unstable cable.

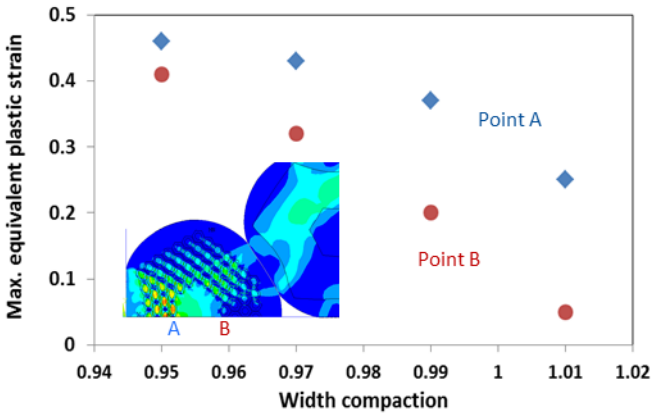

Fig. 22. Maximum equivalent plastic strain in points A and B of edge strand vs. cable width compaction for a 40-strand rectangular cable with edge compaction t_c of 0.92 [110].

<u>*Odd vs even strand number*</u>. The effect of even and odd number of strands in a cable of same cross section was evaluated in [102] using two keystoned Nb-Ti cables with 27 and 28 strands of 1 mm in diameter. Comparison of these two cables demonstrated that, although the cable with an odd number of strands has a slightly smaller packing factor, it remained mechanically stable and had a smaller value and variation of the minor edge compaction. The analysis of subelement deformation inside strands at the cable edges demonstrated better results for the cable with odd number of strands, but more statistics would be needed to make this conclusion significant.

C. Cable Fabrication and Quality Control

Rutherford cables are produced using special cabling machines. The design features and parameters of these machines are reported elsewhere [99], [102], [111].

During cabling, attention is paid to the cable wide and narrow surfaces to exclude strand cross overs and sharp edges. The cable width and thickness are measured periodically or continuously to keep their values within the required tolerances, which are usually of ±6 μm for thickness and of ±24 μm for width. Typical variations of nominal cable thickness along the cable length during cable fabrication are plotted in Fig. 23.

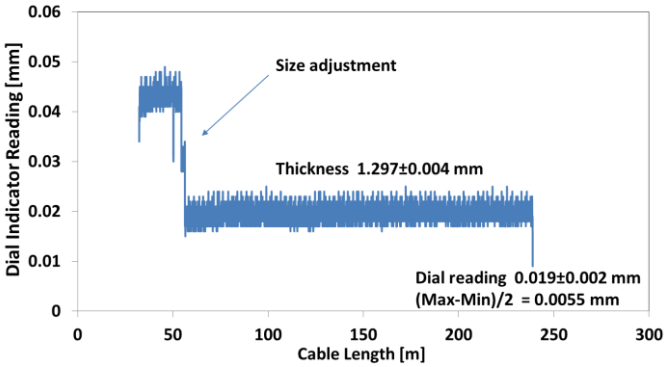

Fig. 23. Typical variations of cable thickness along the length of a Rutherford cable.

D. Cable Size Change After Reaction

It is known that Nb-Sn composite strands expand after reaction due to formation of the Nb_3Sn A15 phase. Whereas in round strands this expansion is isotropic, an anisotropic volume expansion was observed for Nb_3Sn Rutherford cables [112]. While the cable width did not change significantly, the thickness increased by more than expected. To check the hypothesis that the plastic deformation imparted during cabling would release itself through heat treatment, Nb_3Sn strands of different technologies were flat-rolled down to various sizes. The thickness expansion was always larger than the width expansion for both strands and cables. Furthermore, the amount of volume expansion appeared to depend on the strand technology and to be a function of the Nb-Sn content.

The change in dimensions before and after reaction was more recently measured for keystoned cables based on state-of-the-art RRP® strands used in 11 T dipoles [97] and LARP quadrupole models [113]. The average width expansion was 2.6%, the average mid-thickness expansion was 3.9%, and the average length decrease was 0.3%. Some typical LARP cables were reacted under two different conditions: “unconfined” and “confined.” In the first case, the cable is left free to expand or contract in all directions. In the “confined” case, the cable is locked transversally but allowed to freely expand longitudinally. Unlike the individual strands, the “unconfined” cable tests showed a clear longitudinal contraction. The 2-pass cables contracted by about 0.1 to 0.2% whereas the 1-pass cables by about 0.2 to 0.3%. The thickness and the width increased by 1.4% to 4% and by 1.5% to 2% respectively, without any definite correlation to the way the cable was fabricated. When “confined”, the cables elongated by about 0.4% and the thickness increased by about 2%. The width does not change due to the nature of the confinement.

For the purpose of magnetic design optimization, it is the reacted thickness and width values which need to be included in the cable dimensions. The coil dimensions in the winding and curing tooling are determined by the unreacted cable cross section, whereas the coil dimensions in the reaction and impregnation tooling are based on the reacted cable cross section.

V. Nb_3Sn Rutherford Cables Properties

In this section, we detail those key research activities and methods used in the International community that helped study and solve most of the aspects required of Nb_3Sn cables for magnet realization. This includes I_c measurements at high and low fields, flux jump instabilities, effect of cabling deformation on I_c, J_A, *RRR* and stability, effect of transverse pressure on I_c, and interstrand contact resistance.

A. *Cable I_c Measurements*

I_c evaluation of Rutherford cables is performed by either testing short cables samples or individually strands extracted from cables before HT. The good correlation of cable and extracted strand test results, as shown for instance in Fig. 24, confirms the validity of both approaches. The keystoned cable sample, whose results are shown in Fig. 24, was made of 40 RRP® Nb_3Sn strands and was heat treated together with witness samples of its extracted strands. Closed symbols represent I_c data measured in a smooth voltage-current transition, whereas open symbols denote the maximum current I_q as reached before an abrupt quench due to instabilities. Self-field corrections were applied in this plot to both cable and strand test results. A good correlation between extracted strand and cable test results demonstrates also the small variation of strand properties within the different RRP® billets used to make the cable, and confirms a uniform transport current distribution during a cable test. The solid line represents the $I_c(B)$ dependence based on parametrization [29].

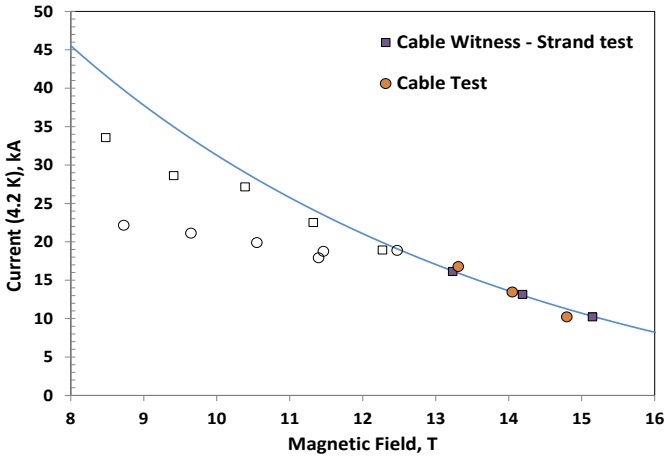

Fig. 24. Cable quench current vs. magnetic field for an insulated Nb_3Sn cable sample made of 40 RRP® Nb_3Sn strands [74].

B. *Flux Jump Instabilities in Cables*

Flux jump instabilities observed in Nb_3Sn strands were seen also in cable short samples. Short cable samples made of different Nb_3Sn strands were tested at FNAL in self-field at 2 K to 4.3 K using a 28 kA SC transformer [114], at BNL in external magnetic fields up to 7 T at 4.3 K, and at CERN in external magnetic fields up to 10 T at 1.8 K to 4.2 K [115]. An excellent correlation of experimental data for similar samples tested at the three different test facilities was found [116].

Analysis and comparison of flux jump instabilities in Rutherford cables and corresponding round wires show (Fig. 25) that these instabilities are larger in cables than in round wires due to subelement deformations and possible subelement merging (Fig. 18), which lead to an increase of $d_{eff.}$. The reduction of strand *RRR* after cabling (see *Section D* below) also increases flux jump instabilities in cables with respect to virgin wires.

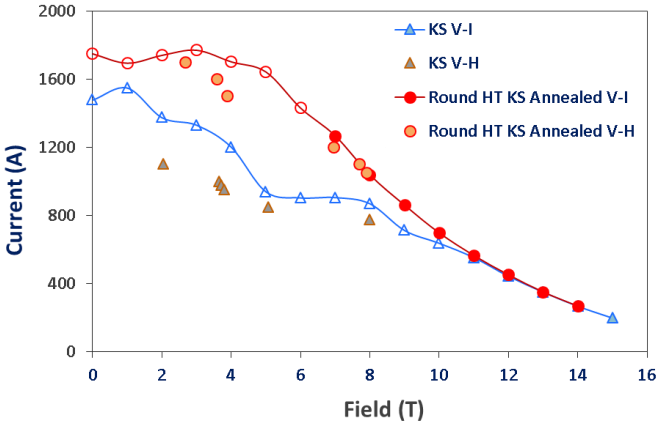

Fig. 25. Instabilities in round wires and extracted strands [117].

The response of a strand to deformation during cabling can be simulated by flat-rolling round wires [118]. This method allows to impart homoneously along a wire the levels of deformation typically associated to the cable edges, and therefore to perform systematic studies of the resulting effects on the conductor. Fig. 26, for instance, shows the magnetization at 12 T field of 1 mm RRP® and PIT deformed wires, parallel to their flat surface, normalized to that of the round strand as a function of wire deformation. Whereas in the PIT samples the magnetization of increasingly thinner strands decreases as expected, in the RRP® samples the magnetization amplitude decreases down to 20% deformation, but starts increasing in a random manner above this threshold. The thorough study in [119] confirmed these and other findings, and explained them in details. In particular, sophisticated magneto-optical imaging clearly proved the electromagnetic fusing of the merged subelements.

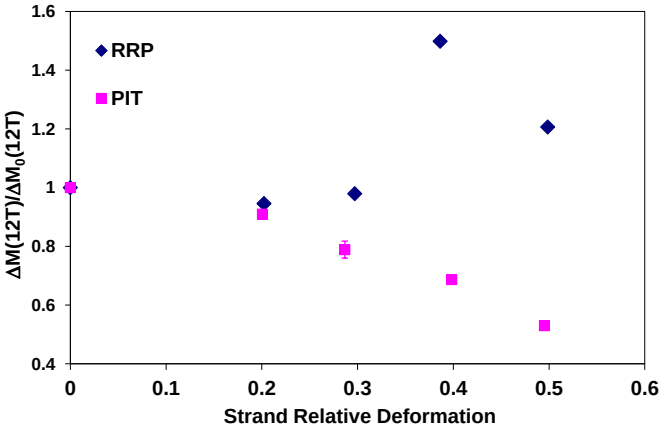

Fig. 26. Magnetization at 12 T field, parallel to the flat surface of a deformed wire, normalized to that of the round strand vs. relative deformation for 1 mm RRP® and PIT wires [118].

C. *Effect of Cable Plastic Deformation*

The effect of cable plastic deformation on the critical current I_c, average critical current density J_A, minimal stability curent I_S and matrix *RRR* was studied using extracted strands [120]. The results of I_c measurements made on extracted strands were compared with those made on round strands used in cables. The cable I_c at 4.2 K and 12 T normalized to the I_c of a cable made of undeformed round strands (*PF*=78.5%) is plotted in Fig. 27 (top) as a function of cable *PF*. Some early IT strands demonstrated relative I_c degradation up to 80% at *PF*s above 84%. A large I_c degradation was also observed in early PIT strands [120]. However, after strand optimization, in particular by increasing the subelement spacing in RRP® strands and by using round filaments in PIT strands, the I_c degradation was reduced to 15% or less at *PF*s up to 94%. At a *PF* between 84 and 87%, which is typical for Nb_3Sn Rutherford cables, the I_c degradation in well optimized cables is usually ~5% or less.

Fig. 27 (bottom) shows the normalized average critical current density J_A as function of cable *PF*. It can be seen from both plots in figure that for all Nb_3Sn strand technologies, the average J_A has an almost flat behavior with *PF* and is larger than in the undeformed cable when the I_c degradation is less than the reduction of cable cross section. Similar measurements performed on cables made with modern RRP® and PIT strands are consistent with these data.

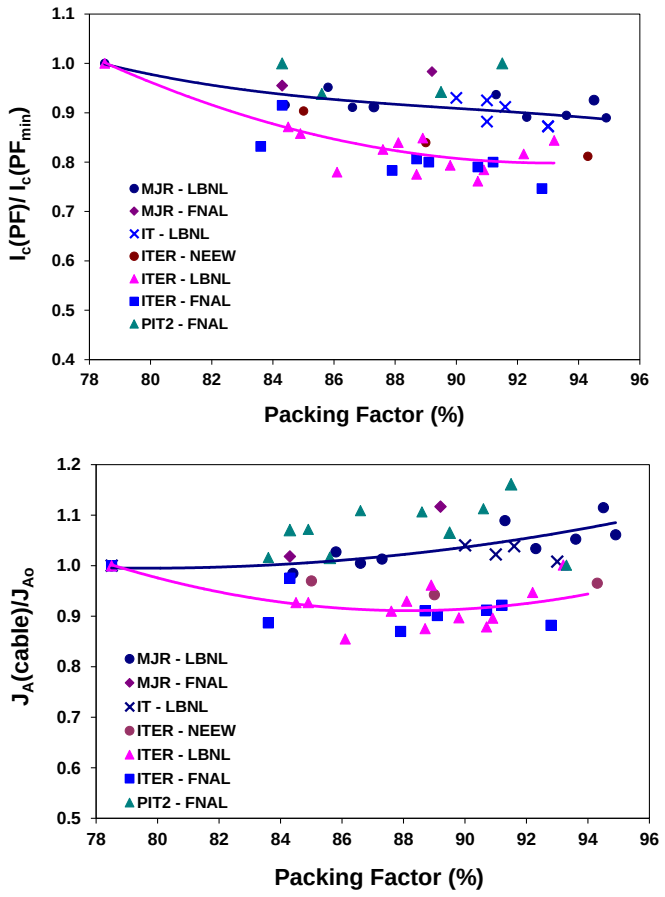

Fig. 27. Normalized cable I_c (top) and normalized average J_A (bottom) at 4.2 K and 12 T vs. *PF* for cables made with IT, MJR and PIT Nb_3Sn strands [120].

It was found that the effect of cabling on the stability current I_S and on the *RRR* is however much stronger than on the I_c, and that subelement damage in a cable is best seen through I_S degradation of its extracted strands [121]. This was confirmed by a cabling study [118] performed to compare the behavior in keystoned cables over an ample *PF* range of an RRP® strand with 50% increased Cu spacing between subelements (called RRP1) with respect to the standard RRP® wire (called RRP2). The I_S at 4.2 K and the *RRR* vs. cable *PF* are plotted in Figs. 28 and 29. The I_S and *RRR* measured values of extracted strands are not as reproducible as in round strands. However, it was shown that the RRP® strand with extra spacing between subelements was able to maintain a higher I_S in the higher *PF* range (above 90%). This indicated that using the improved conductors affords more flexibility for cables ideal to magnet technology, for which larger keystone angles and larger average cable J_A's are desirable.

Based on the results of I_c degradation in Nb_3Sn Rutherford cables, high *PF* values of 92 to 95% provide the highest J_A. However, large I_S and *RRR* degradation due to large deformations and possible damage and merging of the delicate subelements impose an optimal *PF* within 84 to 87%.

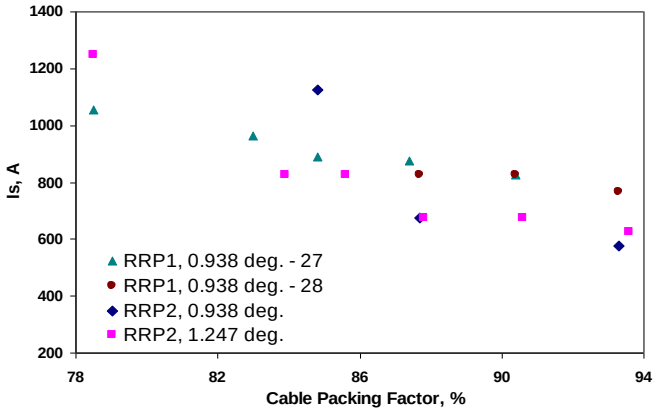

Fig. 28. I_S at 4.2 K as a function of cable packing factor for RRP® strands. RRP1 in legend represents a wire with 50% increased Cu spacing between subelements with respect to a standard RRP® wire called RRP2 [103].

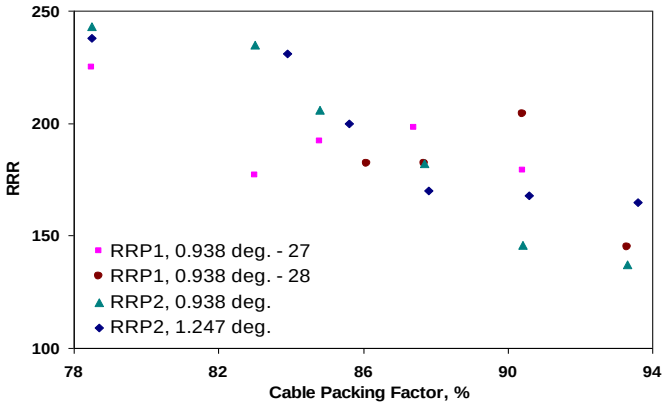

Fig. 29. *RRR* as a function of cable packing factor for RRP® strands. RRP1 in legend represents a wire with 50% increased Cu spacing between subelements with respect to a standard RRP® wire called RRP2 [103].

D. *RRR Variation Along a Strand*

Due to the larger strand deformation at the cable edges, it was expected that *RRR* varied along a strand. Longitudinal variations of *RRR* were estimated from multiple-tap measurements along the length of strands extracted from cables [122]. Voltage taps were placed across straight sections and across the bends of extracted strands (Fig. 30). Resistivity measurements made on extracted strands showed significant *RRR* degradation from the *RRR*≈116±17 for strand segments on the cable faces. On the edges the results were an order of magnitude smaller, *RRR*≈13±5, consistently with local Sn leakages through the diffusion barriers caused by the strong deformation at the cable edges. The average value obtained for a strand when using voltage taps far apart is still large 81±21, due to the localization of the highly deformed edge region. Cables with lesser degradation have been fabricated. However, such large *RRR* degradation at the edges is often found even in cables with low packing factors, and does not seem particularly sensitive to details of edge compaction.

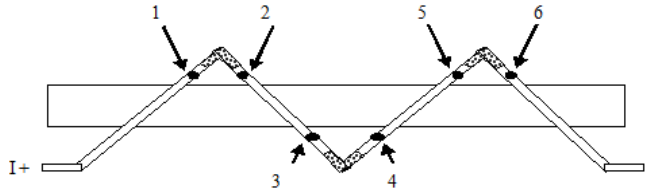

Fig. 30. *RRR* sample configuration. Points 1-6 are voltage taps, Measurements taken between 1-2, 3-4, and 5-6 measure *RRR* as the strand bends over the cable edges, while measurements between 2-3 and 4-5 measure the "straight" sections of the strand on the cable faces [122].

US-LARP and CERN have also been engaged in looking at local *RRR* for the past year and have found that for the cable used in LARP 150-mm quadrupole models QXF the degradation in *RRR* can be up to 40% with respect to that measured in the straight section. Similar patterns were found also in LARP 120-mm quadrupole HQ and 90-mm quadrupole LQ cable (in some cases the reduction of *RRR* was as large as 50%). To maintain a sufficient margin in local *RRR*, the specification for the Hi-Lumi strand *RRR* has been raised to a minimum of 150. In production the edge *RRR* for the Hi-Lumi cable will be monitored [123].

E. *Effect of Transverse Pressure*

Transverse stress is the largest stress component in accelerator magnets up to high magnetic fields. Studies were performed by applying pressure to impregnated cable samples or by testing individual strands inside the cable structure [124]-[127]. Fig. 31 shows examples of I_c sensitivity at 4.2 K of IT (IGC), PIT (SMI), MJR (Teledyne Wah Chang Albany, TWCA) and RRP® (OST) strands to transverse pressures up to 210 MPa measured at FNAL at 12 T [127], and at the University of Twente, the National High Magnetic Field Laboratory [14], and at CERN [128] at 11 and 180.12 T.

Within the limited statistics, there are indications that cables made of high-J_c strands are more sensitive to transverse pressure than those made with older, lower J_c strands. Also, it is possible that a stainless steel core inside the cable reduces pressure sensitivity. It should be noted that the FNAL data represent the effect of uni-axial and not multi-axial strain, since the experimental setup allows for the sample to expand laterally, which produces the largest strain values. In [127], the setup reproduces the uni-axial load case A, represented in Fig. 32 (left), which has $\sigma_{yy} = -p$ and $\sigma_{xx} = \sigma_{zz} = 0$. The second load case, multi-axial case B, represented in Fig. 32 (right), has $\sigma_{yy} = -p$, $\sigma_{xx} = -\nu p$ and $\sigma_{zz} = 0$. Whichever equivalent stress or strain model is used, it is straightforward to verify that load case A always sees strain values larger or at best equal to those produced in load case B.

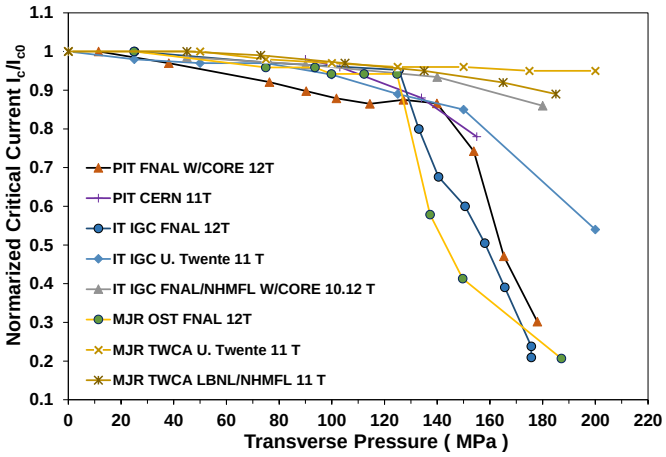

Fig. 31. Normalized I_c(4.2K) vs. transverse pressure on Rutherford cable face for a number of Nb_3Sn conductors measured at FNAL [127], the University of Twente, the National High Magnetic Field Laboratory [14] and CERN [128].

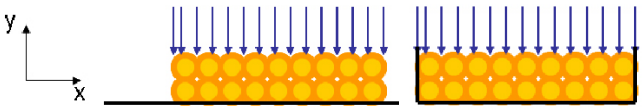

Fig. 32. Uni-axial case A, free sides (left), and multi-axial case B (right).

F. *Interstrand Resistance*

Direct measurements of R_c and R_a contact resistances performed under transverse pressure in [129] gave R_c=1.1 to 1.4 μΩ and R_a=8 to 16 μΩ (10 to 100 MPa) for uncored cables, and R_c=150 to 275 μΩ and R_a=1.5 to 1.9 μΩ (10 to 100 MPa) for cables with a 0.025 mm stainless steel (SS) core. For comparison, in LHC NbTi cables R_c is about 10 to 20 μΩ [130], which is more than 10 times larger than in a Nb_3Sn cable without a resistive core and more than a order of magnitude lower than in a Nb_3Sn cable with resistive core.

Similarly low R_c values of ~0.1 to 0.4 μΩ, measured in Nb_3Sn Rutherford cables reacted in coil under pressure, are reported in [131]-[135]. In cables with a full-width SS core, an excessively high R_c of 246 μΩ was measured. The contact resistances in cable samples were determined based on AC loss measurements.

A special technique to measure interstrand contact resistances in magnet coils was developed at FNAL [136]. The results of measurements in pole and midplane turns of a dipole coil have shown that the adjacent contact resistances were uniform in azimuthal and radial directions, and quite low, i.e. from 0.8 to 4.3 μΩ, providing good conditions for current

sharing in the cable. The range of crossover resistances R_c and variations in the azimuthal direction were instead rather large. R_c changed from 4.4 to 4.5 μΩ in pole turns to 20 to 30 and higher in the midplane turns of both layers.

Studies of interstrand contact resistances in Nb_3Sn Rutherford cables have shown that using a stainless steel core is very efficient in reducing the level of eddy current effects (magnetization, AC loss) in cables. It also helps to reduce the observed variations of contact resistances in Nb_3Sn coils.

VI. Next Steps and R&D Goals

State of the art Nb_3Sn strands and Rutherford cables allow accelerator magnets with nominal operation fields of 10 to 11 T and up to 20% field margin for reliable operation in accelerators. The first Nb_3Sn 11 T dipoles and 150 mm aperture quadrupoles are planned to be installed in the LHC to improve the machine collimation system and achieve higher luminosity [45]. The new post-LHC hadron colliders, whose feasibility studies have started recently in US, EU and China, need more powerful magnets with nominal operation fields ~15 to 16 T [137] and up to 20% margin, bringing the design field to the level of 18 to 19 T.

The maximum design field B_{max} in accelerator magnets is proportional to the critical current density J_c at B_{max} and to the coil width w:

$$B_{max} \sim J_c(B_{max}) \cdot w.$$

Based on this formula, higher fields in accelerator magnets can be achieved by using materials with higher J_c and/or wider coils. Each option has limitations to be taken into consideration, such as higher stress level and storage energy, superconductor and magnet cost, etc.

Target parameters of Nb_3Sn wires for the next generation of accelerator magnets with B_{op}~15 to 16 T are under discussion [138]. Below we describe some R&D directions which are important to achieve target fields of 15 to 16 T with the required margin and to reduce the cost of Nb_3Sn accelerator magnets.

A. Critical Current Density

With the present level of J_c of ~2.5 to 3 kA/mm^2 at 12 T and 4.2 K, a 16 T design field requires a coil width of ~60 mm. A design field of 18 to 19 T, to provide margin during operation at 15 to 16 T, would require a coil thickness increased to 150 mm at least. To reduce the coil volume (i.e. magnet cost), 3 T margin could be provided by increasing the J_c in 60 mm wide coils to ~2 kA/mm^2 at 15 T, which corresponds to ~3.8 kA/mm^2 at 12 T. It is thought that this modest J_c increase can be achieved by further optimization of subelement architecture and Sn content, and by improving its diffusion to the peripheral Nb filaments inside the subelements.

More substantial improvements of Nb_3Sn J_c at high fields, by a factor of 2 or more, would also be desirable to increase reliability and reduce the accelerator magnet cost. This will require significant enhancement of pinning in Nb_3Sn commercial wires. For instance [66] predicts that the $J_c(12T,4.2K)$ of Nb_3Sn could be improved by a factor of 4 to 5 by increasing the transverse flux pinning contribution (typical of Nb-Ti) with respect to the longitudinal one that prevails in current Nb_3Sn materials. This would however require nano-engineering of the material and large effort investments. Another well-known method to improve J_c in Nb_3Sn is by enhancement of the pinning centers density through grain refinement or by the inclusion of engineered pinning centers. Both these options, though demonstrated on laboratory samples using thin films [58], [139] and mono-core wires [51], have yet to be validated in commercial wires.

B. Strand Diameter

The larger coil width in the 15 T class magnets with 50 to 60 mm aperture requires more layers and more turns, and thus leads to larger inductance. The increase of cable width with the present strand diameter of 0.7 to 1.0 mm is restricted by the cable mechanical stability, which significantly reduces with further increases of the cable aspect ratio. The opposing needs of cable width and mechanical stability can be resolved by using strands with larger diameter. Strands with D=1.2 to 1.8 mm are needed for stable cables with aspect ratios of 17 to 12 respectively. Possible restrictions on strand diameter from self-field stability criteria, as well as difficulties with higher cable bending rigidity, could be resolved by using 6-around-1 strand cables based on 0.5 to 0.6 mm Nb_3Sn composite wires. This approach also allows optimizing the Cu cross section area by combining Nb_3Sn and pure Cu wires. A drawback is the reduction of cable packing factor.

C. Subelement Size

The increase of J_c in new strands, required to achieve higher target fields, is a strong incentive to keep d_{eff} under control to avoid premature quenches, field quality degradation at injection, field harmonics fluctuations, and voltage spikes. A d_{eff} of 40 μm or less is still a sound objective. In larger diameter strands it will lead to new strand architectures with larger number of subelements.

D. Cu Stabilizer

To provide reliable protection during a quench, 15 T magnets may need a larger cross section of Cu stabilizer. Increasing the Cu cross section in a composite Nb_3Sn wire may be limited by the wire design and fabrication process. It is also considered as a more expensive approach than adding Cu to the cable cross section. Several options have been proposed and studied [140]-[142]. R&D of large Nb_3Sn cables with large Cu fraction needs to continue.

E. RRR

The *RRR* of the Cu stabilizer is an important parameter for conductor, cable and magnet stability as well as for cable and magnet processing control. Since magnetic field and cabling significantly reduce the Cu matrix *RRR*, wire stability has to be provided by small d_{eff}. On the basis on its sensitivity to deformation, *RRR* should be mostly used as a quality control parameter during cable and magnet processing.

F. Specific Heat

Accelerator magnets made of state-of-the-art Nb_3Sn strands unveil relatively long training. This could be due to the low stability of high-J_c Nb_3Sn wires to flux jumping provoked by

mechanical perturbations in the magnet coils or by epoxy cracking. Conductor stability to flux jumps can be increased by reducing the superconductor filaments size while maintaining low resistivity of the copper matrix, and by increasing the composite specific heat. A considerable increase in stability of Nb_3Sn multifilamentary composite wires produced using the bronze process and internally doped with 7vol.% of PrB_6 was demonstrated in [143]. This important R&D work needs to continue using high-J_c IT and PIT composite wires.

VII. Summary

High-performance composite wires and Rutherford cables are key components of superconducting accelerator magnets. Whereas Nb-Ti has been the workhorse for HEP applications for the past 40 years, Nb_3Sn wires and cables have made exceptional progress and have approached the necessary maturity to be used in accelerator magnets. The advances in Nb_3Sn composite wire and Rutherford cable technologies during the past decade make it possible for the first time to consider Nb_3Sn accelerator magnets with nominal fields up to 12 T in present, e.g. the planned LHC upgrades, and future machines.

This work will continue to achieve the limits of the Nb_3Sn technology. The main goal of Nb_3Sn superconducting wire and cable R&D programs is to understand and improve scientific and engineering aspects of Nb_3Sn strands and cables that are used to make accelerator magnets. The outcome of this effort provides conductor specifications and essential engineering data for design and construction of accelerator magnets. Coordination with industry has been and remains critical to improve performance of commercial Nb_3Sn strands and cables, and international collaboration between laboratories and universities has provided fundamental understanding at all levels.

Acknowledgment

The authors thank J. Parrel, M. Fields (OST), M. Thoener (Bruker EAS), A. Ballarino, B. Bordini, L. Bottura (CERN), A. Kikuchi (NIMS, Japan), A. Ghosh (BNL), M. Sumption (OSU), D. Turrioni (FNAL), T. Wong (Supercon), L.R. Motovidlo (SupraMagnetics), M. Tomsic, Xuang Peng (Hyper Tech), T. Pyon (Luvata), N. Cheggour (NIST) and J. McDonald (US Army Research Laboratory) for their help in preparation of this review.

References

[1] http://www.superconductors.org
[2] *Superconductor Material Science*, S. Foner, B. B. Schwartz, Plenum Press, N. Y., (1981).
[3] B. T. Matthias, T. H. Geballe, S. Geller, and E. Corenzwit, Phys. Rev. 95, 1435 (1954).
[4] J. E. Kunzler, E. Buehler, F. S. L. Hsu and J. H. Wernick, Phys. Rev. Lett. 6, 89 (1961).
[5] K. Tachikawa and Y. Tanaka, Japan. J. Appl. Phys. 5, 834 (1966).
[6] A. R. Kaufman and J. J. Pickett, Bull. Am. Phys. Soc. 15, 833 (1970).
[7] K. Tachikawa, Int. Cryo. Engin. Conf., Berlin (1970); Iliffle Sci. Tech. Pub. 339 (1971).
[8] S. Wolff, "Review of Accelerator Magnet Design in the World," IEEE Trans. on Mag., vol. 28, no.1, 1992, p. 96.
[9] N. Mitchell et al., "Conductor designs for the ITER toroidal and poloidal magnet systems," IEEE Trans. on Mag., 1994, p. 1602.
[10] J. A. Parrell, M. B. Field, Y. Zhang, and S. Hong, Adv. Cryo. Eng. (Materials) 50B, 369 (2004).
[11] J. H. Lindenhovius et al., "Progress in the Development of Nb_3Sn Conductors based on the "Powder in Tube" Method with Finer Filaments," IEEE Trans. Appl. Supercond, 9, 1451 (1999).
[12] A. Godeke, A. den Ouden, A. Nijhuis, and H. H. J. ten Kate, Cryogenics 48, 308 (2008).
[13] A. Godeke, "A review of the properties of Nb_3Sn and their variation with A15 composition, morphology and strain state", Supercond. Sci. Technol. 19 (2006) R68–R80.
[14] D. R. Dietderich, A. Godeke, "Nb_3Sn research and development in the USA – Wires and cables", Cryogenics 48, 331 (2008).
[15] L. Bottura and A. Godeke, "Superconducting materials and conductors, fabrication, and limiting parameters," Reviews of Accelerator Science and Technology, 5 (2012), p. 25.
[16] M. N. Wilson, "Superconducting Magnets for Accelerators: a Review," IEEE Trans. Appl. Supercond., Vol. 7, No. 2, June 1997, p. 727.
[17] G. Gallagher-Daggit, Superconductor cables for pulsed dipole magnets. Technical report (Rutherford Laboratory Memorandum No. RHEL/M/A25, 1973).
[18] S. A. Gourlay, "High Field Magnet R&D in the USA," IEEE Trans. Appl. Supercond., Vol. 14, No.2, June 2004, p.333.
[19] A. Devred et al., "High field accelerator magnet R&D in Europe," IEEE Trans. Appl. Supercond., vol. 14, no. 2, pp. 339–344, 2004.
[20] M. N. Wilson, Superconducting Magnets, Oxford University Press, New York, 1983.
[21] Y. Hashimoto, K. Yoshizaki, and M. Tanaka, Proc. of 5th Internat. Cryo. Eng. Conf., Kyoto, Japan (1974), p. 332.
[22] J. C. McKinnell et al, "Fully bonded Internal-Tin, Niobium-Tin (Nb_3Sn) conductor development at Oxford Superconducting Technology," IEEE Trans. Appl. Supercond., Vol. 7, p1360, 1997.
[23] M. Wake et al., "Development of high current density Nb_3Sn conductor with distributed tin configuration," Adv. Cryo. Eng., vol. 50B, pp. 410–416, 2004.
[24] M. Durante et al., "Development of a Nb_3Sn multifilamentary wire for accelerator magnet applications," Physica C, vol. 354, p. 449, 2001.
[25] S. Mattafirri et al., "Kinetics of Phase Growth in the Cu-Sn System and Application to Composite Nb_3Sn Strands", IEEE Trans. Appl. Sup., V. 13, No. 2, p. 3418 (2003).
[26] J.-M. Rey et al., "Effect of Partially Reacting Nb_3Sn Before Magnet Winding on the Strand Critical Current", Advances in Cryogenic Engineering, V. 48, AIP, V. 614, pp. 1001-1007 (2002).
[27] A.K. Ghosh et al., "Systematic Changes of the Nb-Sn Reaction with Time, Temperature, and Alloying in Restacked-Rod-Process (RRP) Nb_3Sn Strands," IEEE Trans. Appl. Supercond., Vol. 19, No. 3, June 2009, p. 2580.
[28] T. Boutboul et al., "Heat Treatment Optimization Studies on PIT Nb_3Sn Strand for the NED Project," IEEE Trans. Appl. Supercond., Vol. 19, No. 3, June 2009, p. 2564.
[29] L.T. Summers et al., "A model for the prediction of Nb_3Sn critical current as a function of field, temperature, strain and radiation damage", IEEE Trans. on Magnetics, 27 (2): 2041-2044 (1991).
[30] D.M.J. Taylor, D.P. Hampshire, "The Scaling Law for the Strain Dependence of the Critical Current Density in Nb_3Sn Superconducting Wires," Superconductor Science and Technology, **18**, S241-S252, 2005.
[31] A. Godeke et al., "A General Scaling Relation for the Critical Current Density in Nb_3Sn," Superconductor Science and Technology, **19**, R100-R116, 2006
[32] J.W. Ekin, "Experimental Techniques for Low-Temperature Measurements", OXFORD University Press, pp. 461-463. Oxford University Press, New York, Reprinted 2007.
[33] V.V. Kashikhin and A.V. Zlobin, "Correction of the Persistent Current Effect in Nb_3Sn Dipole Magnets", IEEE Trans. Appl. Supercond., v. 11, No. 1, March 2001, p. 2058.
[34] W. J. Carr, J. Appl. Phys., 45, 1974, p.935.
[35] L.D. Cooley, A.K. Ghosh and R.M. Scanlan, "Costs of high-field superconducting strands for particle accelerator magnets", Supercond. Sci. Technol. 18 (2005) R51–R65.
[36] R. M. Scanlan, "Conductor Development for High Energy Physics-Plans and Status of the U. S. Program", IEEE Trans. Appl. Supercond., vol. 11, No. 1, March 2001, p. 2150.

[37] R. M. Scanlan, D.R. Dietderich, "Progress and Plans for the U.S. HEP Conductor Development Program", IEEE Trans. Appl. Supercond., vol. 13, No. 2, June 2003, p. 1536.

[38] T. Pyon et al., "Development of High Performance Nb3Sn Conductor for Fusion and Accelerator Applications," IEEE Trans. Appl. Supercond., Vol. 17, No. 2, June 2007, p. 2568.

[39] G. J. Peters et al., "The DOE High Energy Physics SBIR/STTR Superconductivity Program", IEEE Trans. Appl. Supercond., vol. 13, No. 2, June 2003, p. 1520.

[40] J. L. H. Lindenhovius et al., "Powder-in-tube (PIT) Nb_3Sn conductors for high field magnets," IEEE Trans. Appl. Supercond., vol. 10, no. 1, pp. 975–978, March 2000.

[41] A. Kikuchi, private communication

[42] D.R. Dietderich, A. Godeke, "Nb_3Sn research and development in the USA – Wires and cables", Cryogenics 48, 331 (2008).

[43] M.B. Field et al. "Optimizing Nb_3Sn Conductors for High Field Applications," IEEE Trans. Appl. Supercond., Vol. 24, No. 3, June 2014, 6001105.

[44] Cheggour N et al., Supercond. Sci. Technol. 23 (2010) 052002.

[45] L. Bottura et al., "Advanced Accelerator Magnets for Upgrading the LHC," IEEE Transactions on Applied Superconductivity, vol. 22, no. 3, 2012, 4002008.

[46] C.V. Renaud, L.R. Motowidlo, T. Wong, "Status of powder-in-tube Nb_3Sn conductor development at Supercon," IEEE Trans. Appl. Supercond., Vol. 13, No. 2, 2003, p.3490.

[47] C.V. Renaud, T. Wong, "Titanium Doped Nb_3Sn Superconductor Fabricated by the Internal Tin Tube (ITT) Approach," IEEE Trans. Appl. Supercond., Vol. 19, No. 3, 2009, p.2548.

[48] E. Gregory et al., "A tubular process for making Nb_3Sn conductors," Adv. Cryo. Eng., vol. 54, 2008, p. 252.

[49] E. Gregory et al., "Nb_3Sn superconductors made by an economical tubular process," IEEE Trans. Appl. Supercond., vol. 19, no. 2, 2009, p. 2602.

[50] X. Peng et al., "An Economical Tubular Process for Manufacturing Nb_3Sn Superconductors," IEEE Trans. Appl. Supercond., Vol. 21, No. 3, 2011.

[51] X. Xu, M.D. Sumption, X. Peng, "Internally Oxidized Nb_3Sn Strands with Fine Grain Size and High Critical Current Density", Adv. Mater. 2015, 27, 1346–1350.

[52] L.R. Motowidlo, G.M. Ozeryansky, "A New PIT Nb_3Sn Conductor for High Magnetic Field Applications," IEEE Trans. Appl. Supercond., Vol. 18, No. 2, 2008, p.1001.

[53] L.R. Motowidlo et al., "New Developments in Nb_3Sn PIT Strand: The Effects of Titanium and Second Phase Additions on the Superconducting Properties," IEEE Trans. Appl. Supercond., Vol. 21, No. 3, 2011, p.2546.

[54] J.J. Hanak and R. E. Enstrom, Proc. of the 10th International conference on Low Temperature Physics, Moscow, p. 10 (1966).

[55] C.S. Pande and M. Suenaga, Appl. Phys. Letters 29, 443 (1976).

[56] A.W. West and R.D. Rawlings, J. Mater. Sci. 12, 1862 (1977).

[57] P.E. Madsen and R.F. Hills, IEEE Trans. on Magnetics MAG-15, 181 (1979).

[58] D.R. Dietderich et al., "High critical current densities in Nb3Sn films with engineered microstructures – artificial pinning microstructures", Adv Cryo Eng (Mater) 1998; 44:951.

[59] D. Dew-Hughes, *Phil. Mag. B*, vol. 55, No. 4, pp. 459-479, 1987.

[60] E. J. Kramer, *J. Appl. Phys*., vol. 44, No. 3, pp. 1360-70, March 1973.

[61] M. Suenaga, K. Tsuchiya, N. Higuchi, and K. Tachikawa, *Cryogenics*, vol. 25, pp. 123-8, 1985.

[62] J. E. Evetts and C. J. Plummer, *Proc. Int. Symp. on Flux Pinning and Electromagnetic Properties in Superconductors,* edited by T. Matsushita, K. Yamafuji, and F. Irie, Fukuoka: Matsukuma, 1985, p. 146.

[63] D. F. Hampshire, H. Jones, and E. W. J. Mitchell, *IEEE Trans. Mag.*, vol. 21, pp. 289-92, 1985.

[64] W. Schauer, and W. Schelb, *IEEE Trans. Mag.*, vol. 17, pp. 374-377, 1981.

[65] R. Taillard and A. Ustinov, "Evolutions of grains during the heat treatments of internal-tin Nb_3Sn," *Adv. Cry. Eng.*, vol. 46B, 2000.

[66] J. McDonald et al., "A Model for J_c in Granular A-15 Superconductors", IEEE Trans. Appl. Sup., V. 11, No. 1, p. 3884 (2001).

[67] E. Barzi et al., "Superconductor and Cable R&D for High Field Accelerator Magnets at Fermilab", IEEE Trans. Appl. Supercond., Vol. 12, No. 1, p. 1009 (2002).

[68] M. Field, private communication.

[69] E. Barzi, E. Gregory, T. Pyon., "Heat Treatment Optimization of Internal Tin Nb_3Sn Strands", IEEE Trans. Appl. Supercond., Vol. 11, No. 1, p. 3573 (2001).

[70] E. Barzi et al., "Nb_3Sn Phase Growth and Superconducting Properties during Heat Treatment", IEEE Trans. Appl. Supercond., V. 13, No. 2, p. 3414 (2003).

[71] A. K. Ghosh, L. D. Cooley, and A. R. Moodenbaugh, "Investigation of instability in high J_c Nb_3Sn strands," IEEE Trans. Appl. Supercond., vol. 15, no. 2, pp. 3360–3363, Jun. 2005.

[72] Lim K C, Thomson J D, and Webb G W. "Electronic density of states and T_c in Nb_3Sn under pressure", Phys Rev B 1983; 27: 2781-2787.

[73] Li Qiao, Lin Yang and Jie Song, CRYOGENICS-D-14-00136R1 (2015).

[74] E. Barzi, D. Turrioni, and A.V. Zlobin, "Progress in Nb_3Sn RRP Strand Studies and Rutherford Cable Development at FNAL", IEEE Trans. Appl. Supercond., Vol. 24, Issue 3, June 2014 Page 6000808.

[75] G. Ambrosio et al., "Study of the React and Wind Technique for a Nb_3Sn Common Coil Dipole", IEEE Trans. Appl. Sup., V. 10, No. 1, p. 338 (2000).

[76] G. Ambrosio et al., "Development of React & Wind Common Coil Dipoles for VLHC", IEEE Trans. Appl. Sup., V. 11, No. 1, p. 2172 (2001).

[77] P. Bauer et al., "Fabrication and Testing of Rutherford-type Cables for React and Wind Accelerator Magnets", IEEE Trans. Appl. Sup., V. 11, No. 1, p. 2457 (2001).

[78] A.V. Zlobin, V.V. Kashikhin, E. Barzi, "Effect of Magnetic Instabilities in Superconductor on Nb_3Sn Accelerator Magnet Performance", IEEE Trans. Appl. Supercond., Vol. 16, Issue 2, June 2006 p. 1308.

[79] H. Brechna, Superconducting magnet systems, Springer, Berlin, 1973.

[80] E. Barzi et al., "Study of Nb_3Sn strands for Fermilab's high field dipole magnets," IEEE Trans. Appl. Supercond., vol. 11, p. 3595, March 2001.

[81] R. B. Goldfarb et al., "Suppression of flux jumps in marginally stable Niobium-Tin superconductors," IEEE Trans. Appl. Supercond., p. 3679, March 2001.

[82] M.D. Sumption et al., "Analysis of magnetization, AC loss, and deff for various internal-Sn based Nb_3Sn multifilamentary strands with and without subelement splitting," Cryogenics, vol. 44, pp. 711–725, 2004.

[83] A. K. Ghosh et al., "Magnetization studies of high J_c Nb_3Sn strands," IEEE Trans. Appl. Supercond., vol. 15, p. 3494, 2005.

[84] E. Barzi, "Superconductor and Cable R&D for High Field Accelerator Magnets at Fermilab", Progress of Nb-Based Superconductors, printed Feb. 18, 2005, by Maeda printing Co., LTD, Editors K. Inoue, T. Takeuchi, A. Kikuchi.

[85] B. Barzi et al., "Instability in transport current measurement of Nb_3Sn Strands," IEEE Trans. Appl. Supercond., vol. 15, p. 3364, 2005.

[86] D. R. Dietderich et al., "Correlation between strand stability and magnet performance," IEEE Trans. Appl. Supercond., vol. 15, p. 1524, 2005.

[87] A.K. Ghosh, "Effect of Copper Resistivity and Filament Size on the Self-Field Instability of High-J_c Nb_3Sn Strands," IEEE Trans. Appl. Supercond., vol. 23, no.3, 2013, 7100407.

[88] R. Hancox, "Enthalpy Stabilized Superconducting Magnets," IEEE Trans. on Magnetics, Vol. MAG-4, Issue 3, September 1968, p. 486.

[89] V.V. Kashikhin, A.V. Zlobin, "Magnetic Instabilities in Nb_3Sn Strands and Cables", IEEE Trans. Appl. Supercond., Vol. 15, Issue 2, June 2005, p. 1621.

[90] M. D. Sumption and E. W. Collings, "Modeling current-field instability in high performance Nb_3Sn strands in moderate field," IEEE Trans. Appl. Supercond., vol. 17, pp. 2714–2717, 2007.

[91] B. Bordini et al., "Self-field effects in magneto-thermal instabilities for Nb-Sn strands," IEEE Trans. Appl. Supercond., vol. 18, p. 1309, 2008.

[92] A.K. Ghosh et al., "Investigation of Instability in High J_c Nb_3Sn Strands," IEEE Trans. Appl. Supercond., Vol. 15, Issue 2, June 2005, p. 3360.

[93] B. Bordini et al., "Impact of the Residual Resistivity Ratio on the Stability of Nb_3Sn Magnets", IEEE Ttans. Appl. Sup., Vol. 22, No. 3, June 2012, 4705804.

[94] S. Moio ,"Effect of Subelement Size, RRR and Strand Size on Stability of RRP Nb_3Sn Strands", Masters Thesis, Turin Polytechnics(2011).

[95] B. Bordini et al., "Voltage spikes in Nb_3Sn and NbTi strands," IEEE Trans. Appl. Supercond., vol. 16, no. 2, pp. 366–369, Jun. 2006.

[96] S. Feher et al., "Sudden Flux Change Studies in High Field Superconducting Accelerator Magnets", IEEE Trans. Appl. Supercond., vol.15, no.2, June 2005, pp 1591 – 1594.

[97] E. Barzi et al., "Development and Fabrication of Nb_3Sn Rutherford Cable for the 11 T DS Dipole Demonstration Model", IEEE Trans. Appl. Supercond., Vol. 22, Issue 3, June 2012 6000805.
[98] M.N. Wilson, Preprint RHEL/M/A26, 1972.
[99] J.D. Adams et al., "Rutherford Cables with Anisotropic Transverse Resistance", IEEE Trans. on Magnetics, Vol. 7, No. 2, June 1997, p. 958.
[100] V.E. Sytnikov, et al., "Coupling current losses in superconducting transposed conductors located in changing magnetic fields," Cryogenics, 2 9, pp. 926-930, 1989.
[101] A. Devred et al., "Interstrand Resistance Measurements on Nb_3Sn Rutherford-Type Cables", IEEE Trans. on Magnetics, Vol. 9, No. 2, June 1999, p. 722.
[102] N. Andreev et al., "Development of Rutherford-type Cables for High Field Accelerator Magnets at Fermilab", IEEE Transactions on Applied Superconductivity, Volume 17, Issue 2, June 2007 Page(s):1027-1030.
[103] D. Turrioni, et al., "Effects of Rutherford Cable Parameters on Nb_3Sn Extracted Strand Deformation and Performance", IEEE Transactions on Applied Superconductivity, Vol. 18, Issue 2, June 2008, p. 1114.
[104] E. Barzi, G. Gallo, and P. Neri, "FEM Analysis of Nb-Sn Rutherford-type Cables", IEEE Trans. Appl. Sup., Vol. 22, Issue 3, June 2012.
[105] S. Farinon et al., "Nb_3Sn wire layout optimization to reduce cabling degradation," IEEE Trans. Appl. Supercond., vol. 17, no. 2, pp. 984–988, Jun. 2007.
[106] M. Alsharoa et al., "Optimization of brittle superconducting Nb_3Sn strand design," IEEE Trans. Appl. Supercond., vol. 18, no. 2, pp. 1496–1499, Jun. 2008.
[107] E. Z. Barzi, M. Bossert, and G. Gallo, "A model to study plastic deformation in RRP Nb_3Sn wires," IEEE Trans. Appl. Supercond., vol. 21, no. 3, pp. 2588–2592, Jun. 2011.
[108] P. Mallon et al., "Mechanical material characterization and finite element modeling of unreacted Nb_3Sn PIT wires under transverse pressure," IEEE Trans. Appl. Supercond., vol. 23, no. 3, Jun. 2013, 8400804.
[109] E. Rochepault et al., "Analysis and Modeling of Damage in RRP Nb_3Sn Wires During Cabling," IEEE Trans. Appl. Supercond., vol. 25, no. 3, Jun. 2015, 8800905.
[110] E. Barzi et al. , "Superconducting strand and cable development for the LHC upgrades and beyond", IEEE Trans. Appl. Sup., V. 23, No. 3, (2013).
[111] J. Grisel et al., "A unique cabling machine designed to produce Rutherford-type superconducting cable for the SSC project," IEEE Trans. on Magnetics, Vol. 25, No. 2, March 1989, p. 1608.
[112] N. Andreev *et al.*, "Volume expansion of Nb_3Sn strands and cables during heat treatment", *Advances in Cryogenic Engineering*, V. 48, AIP, V. 614, pp. 941-948 (2002).
[113] H. Felice, et al., "Impact of Coil Compaction on Nb_3Sn LARP HQ Magnet", IEEE Trans. Applied Supercond., Vol. 22, Issue 3, June 2012. 4001904.
[114] E. Barzi et al., "Study of Nb_3Sn Cable Stability at Self-field Using a SC Transformer", IEEE Trans. App. Supercond., Vol. 15, Issue 2, June 2005 Page(s):1537 – 1540.
[115] G. Ambrosio, et al., "Critical Current and Instability Threshold Measurement of Nb_3Sn Cables for High Field Accelerator Magnets", IEEE Trans. Appl. Supercond., Vol. 15, Issue 2, June 2005, p.1545.
[116] A.V. Zlobin et al., "R&D of Nb_3Sn Accelerator Magnets at Fermilab", IEEE Trans. Appl. Supercond., Vol. 15, Issue 2, June 2005, p. 1113.
[117] E. Barzi et al., "Nb_3Sn Cable Development for the 11 T Dipole Demonstration Model", CEC/ICMC'2011, Spokane, WA, June 2011.
[118] D. Turrioni et al., "Study of Effects of Deformation in Nb_3Sn Multifilamentary Strands", IEEE Trans. Appl. Sup., V. 17, No. 2, p. 2710 (2007).
[119] A. Polyanskii, et al., "Evidence for Highly Localized Damage in Internal Tin and Powder-In-Tube Nb_3Sn Strands Rolled Before Reaction Obtained from Coupled Magneto-Optical Imaging and Confocal Laser Scanning Microscope", Supercond. Sci. Technol. 22 (2009).
[120] E. Barzi et al., "Development and study of Rutherford-type cables for high-field accelerators magnets at Fermilab", Supercond. Sci. Technol. 17 (May 2004) S213-S216.
[121] E. Barzi et al., "RRP Nb_3Sn Strand Studies for LARP", IEEE Trans. Appl. Supercond., V. 17, No. 2, p. 2607 (2007).
[122] M.D. Sumption, et al., "Measurement of RRR variation in strands extracted from Nb_3Sn-type Rutherford cable", CEC/ICMC'07, Chattanooga, TN, July 16-20 2007.
[123] Ghosh, private communication.
[124] J. Van Oort, et al., "The reduction of the critical current in Nb_3Sn cables under transverse loads," IEEE Trans. Appl. Supercond., vol. 3, no. 1, pp. 559–592, Mar. 1993.
[125] G. Pasztor et al., "Transverse stress effects in Nb_3Sn Cables", IEEE Trans. Appl. Supercond., vol. 30, no. 4, July 1994, p.1938.
[126] D. R. Dietderich et al., "Critical current of superconducting Rutherford cable in high magnetic fields with transverse pressure", IEEE Trans. Appl. Supercond., vol. 9, 1999, p. 122.
[127] Barzi, D. Turrioni, and A. V. Zlobin, "Effect of Transverse Pressure on Brittle Superconductors", EIEEE Trans. Appl. Sup., V. 18, No. 2, p. 980 (2008).
[128] B. Bordini et al., "Critical Current Measurements of High-J_c Nb_3Sn Rutherford Cables Under Transverse Compression", IEEE Trans. Appl. Supercond., Vol. 24, Issue 3, June 2014, 9501005
[129] Devred et al., "Interstrand Resistance Measurements on Nb_3Sn Rutherford-Type Cables", IEEE Trans. on Magnetics, Vol. 9, No. 2, June 1999, p. 722.
[130] Z. Ang, et al., IEEE Trans. Appl. Supercond., vol. 9, pp. 735–741, 1999.
[131] E. W. Collings, et al., IEEE Trans. Appl. Supercond., vol. 20, pp. 1387–1390, 2010.
[132] M. D. Sumption, et al., IEEE Trans. Appl. Supercond., vol. 16, pp. 1200–1203, 2006.
[133] M. D. Sumption, et al., Adv. Cryo. Eng. (Materials), vol. 50, pp. 781–788, 2004.
[134] E. W. Collings, et al., IEEE Trans. Appl. Supercond., vol. 17, pp. 2494–2497, 2007.
[135] E.W. Collings et al., "Influence of a Stainless Steel Core on Coupling Loss, Interstrand Contact Resistance, and Magnetization of an Nb_3Sn Rutherford Cable", IEEE Trans. Appl. Supercond., Vol. 18, Issue 2, June 2008, p.1301.
[136] G. Ambrosio et al., "Measurement of Inter-Strand Contact Resistance in Epoxy Impregnated Nb_3Sn Rutherford Cables," CEC/ICMC2003, Alaska, September 22-25 2003.
[137] D. Schulte et al, "Specification: Future Circular Collider Study - Hadron Collider Parameters," EDMS No. 1342402, FCC-ACC-SPC-0001 v.1.0.
[138] A. Ballarino, L. Bottura, "Targets for R&D on Nb_3Sn Conductor for High Energy Physics," IEEE Trans. on Applied Supercond., Vol. 25, Issue 3, June 2015. 6000906.
[139] L.C. Cooley and P.J. Lee, "Shift of the Flux-Pinning Force Curve in Nb_3Sn Thin Films with Very Fine Grain Size," IEEE Trans. Appl. Supercond., Vol. 11, No. 1, March 2001, p. 3820.
[140] V.V. Kashikhin, A.V. Zlobin, "Single-layer high field dipole magnets", Paper RPPH081, PAC'01, Chicago, IL, June 2001, v.5, p.3415.
[141] D.R. Chichili et al., "Fabrication of Nb_3Sn Shell-Type Coils with Pre-Preg Ceramic Insulation", CEC/ICMC 2003, Alaska, September 22-25 2003.
[142] M. Coccoli et al., "Fabrication and Performance of Nb_3Sn Rutherford-Type Cable with Cu Added as a Separate Component," IEEE Transactions on Applied Superconductivity, 14, 2, 2004.
[143] V.E. Keilin et al., "Considerable stability increase of Nb_3Sn multifilamentary wire internally doped with a large heat capacity substance (PrB_6)", Supercond. Sci. Technol. 22 (2009) 085007 (5 pp).